This is the preprint version of the following article: *Vila-Parrondo, C; García-Astrain, C; Liz-Marzán, LM., Colloidal systems toward 3D cell culture scaffolds, Advances in Colloid and Interface Science, 2020, 283 (102237)*
DOI: 10.1016/j.cis.2020.102237

COLLOIDAL SYSTEMS TOWARD 3D CELL CULTURE SCAFFOLDS[+]

Christian Vila-Parrondo[a], Clara García-Astrain[a*], Luis M. Liz-Marzán[a,b,c*]

[a] CIC biomaGUNE, Basque Research and Technology Alliance (BRTA), Paseo de Miramon 182, 20014, Donostia San Sebastián, Spain
[b]Centro de Investigación Biomédica en Red, Bioingeniería, Biomateriales, y Nanomedicina (CIBER-BBN), Paseo de Miramón 182, 20014 Donostia-San Sebastián, Spain
[c] Ikerbasque Basque Foundation for Science, 48013 Bilbao, Spain
** Corresponding Authors: cgarcia@cicbiomagune.es (C. García-Astrain)*
llizmarzan@cicbiomagune.es (L. M. Liz-Marzán)
[+]Dedicated to our friend Ramón González-Rubio

Abstract

Three-dimensional porous scaffolds are essential for the development of tissue engineering and regeneration, as biomimetic supports to recreate the microenvironment present in natural tissues. To successfully achieve the growth and development of a specific kind of tissue, porous matrices should be able to influence cell behavior by promoting close cell-cell and cell-matrix interactions. To achieve this goal, the scaffold must fulfil a set of conditions, including ordered interconnected porosity to promote cell diffusion and vascularization, mechanical strength to support the tissue during continuous ingrowth, and biocompatibility to avoid toxicity. Among various building approaches to the construction of porous matrices, selected strategies afford hierarchical scaffolds with such defined properties. The control over porosity, microstructure or morphology, is crucial to the fabrication of high-end, reproducible scaffolds for the target application. In this review, we provide an insight into recent advances toward the colloidal fabrication of hierarchical scaffolds. After identifying the main requirements for scaffolds in biomedical applications, conceptual building processes are introduced. Examples of tissue regeneration applications are provided for different scaffold types, highlighting their versatility and biocompatibility. We finally provide a prospect about the current state of the art and limitations of porous scaffolds, along with challenges that are to be addressed, so these materials consolidate in the fields of tissue engineering and drug delivery.

Keywords: porous scaffolds, hierarchical materials, inverse opals, tissue engineering, microstructure

Abbreviations

Carbon nanofibers (CNFs)

Chitosan (CS)

Confocal Laser Scanning Microscopy (CLSM)

Critical temperature (T_c)

Critical pressure (P_c)

Embryonic neural progenitor cells (ENCPs)

Ethyl acetate (EA)

Ethyl lactate (EL)

Foaming temperature (T_F)

Graphene oxide (GOx)

Growth Factor (GF)

High Internal Phase Emulsions (HIPE)

Human bone marrow stromal cell (hBMSC)

Human induced pluripotent stem cells derived from neural precursor cells (hiPC-NPCs)

Human mesenchymal stem cells (hMSCs)

Human pluripotent stem cells (hPSC)

Human umbilical vein endothelial cells (hUVECS)

Hydroxyapatite (HAp)

Ice segregation-induced self-assembly (ISISA)

Induced pluripotent stem cells (iPs)

Inverse opal (IO)

Mesenchymal stem cells (MSCs)

Multi-walled carbon nanotubes (MWCNTs)

Neural precursor cells (NPC)

Photonic crystal (PhC)

Polycaprolactone (PCL)

Poly(D,L-lactic-co-glycolic acid) (PLGA)

Polyethylene glycol (PEG)

Polyethylene glycol diacrylate (PEGDA)

Poly (γ-glutamic acid) (γ-PGA)

Polylactic acid (PLA)

Polymethyl methacrylate (PMMA)

Polystyrene (PS)

Polyvinyl alcohol (PVA)

Rat bone marrow-derived mesenchymal stem cells (rBMSCs)

Recombinant human bone morphogenic protein-2 (rhBMP-2)

Supercritical CO_2 ($scCO_2$)

Supercritical fluids (SCFs)

Thermoplastic zein (TZ)

Trimethylolpropane triacrylate (TMPTA)

Vascular endothelial growth factor (VEGF)

Contents

1. INTRODUCTION 5
2. REQUISITES FOR SCAFFOLD DEVELOPMENT 6
3. SCAFFOLD FABRICATION 8
3.1. Inverse Opals 8
3.2. Emulsion Templating 11
3.3. Ice templating 13
3.4. Supercritical Fluids (SCFs) 17
4. POROUS SCAFFOLDS FOR TISSUE ENGINEERING 22
4.1. Bone tissue engineering 23
4.2. Neural cell growth 31
4.3. Cardiac tissue and neovascularization 36
5. CONCLUSIONS AND OUTLOOK 38
DECLARATION OF COMPETING INTEREST 40
ACKNOWLEDGEMENTS 40
REFERENCES 40

1. INTRODUCTION

To truly understand how cell tissues behave, grow and repair themselves, it is essential to create cell models that can reproduce the complex 3D structure found in living beings. However, most studies are based on either *in vitro* two-dimensional (2D) cell cultures or *in vivo* animal models, which fail to reproduce the human cellular microenvironment [1]. Despite the advances obtained through 2D cell cultures, cells grown on a flat surface cannot reproduce the cell-cell and cell-matrix interactions present in 3D living tissues and discrepancies are thus commonly observed when translating the obtained results into clinical trials in humans. Similar discrepancies apply when dealing with animal models that may differ, for example, in terms of stem cell differentiation or therapeutic drug response [2]. Therefore, there is a clear need for the development of 3D cell cultures supported by scaffolds that can promote cell attachment and migration, thereby providing the appropriate biochemical and biophysical cues, and enabling the diffusion of nutrients and oxygen to better mimic living tissues. In order to achieve this goal, the scaffolds need to fulfil a set of requirements that include biocompatibility, reproducibility, high porosity (with specific pore size and interconnectivity), tailored biodegradability, adequate mechanical properties to support tissue growth, and appropriate biochemical functionalities [3].

In this context, appropriate material selection and scaffold fabrication strategies are critical to produce compelling scaffolds for tissue engineering applications. These applications include porous biomedical implants, 3D cell models and *in vivo* tissue-induced regeneration, but may offer additional functionalities such as drug delivery, diagnostics or sensing. Therefore, morphological and microstructural features, as well as degradation time, are to be tailored to the intended application [4]. Ceramic, metallic and polymer-based materials have been widely applied to the preparation of scaffolds for biomedical applications. Resistance against corrosion and high biocompatibility have boosted the use of metallic materials such as titanium, cobalt or magnesium alloys, for dental applications and orthopaedics [5]. Ceramic materials in turn feature high thermal and chemical stability, as well as good mechanical properties for their use as implants, usually being the material of choice for bone tissue engineering. Examples of these materials include alumina, zirconia, bioactive glass, tricalcium phosphate and,

their greatest exponent for bone engineering, hydroxyapatite [6]. Finally, biocompatible polymers of both natural (i.e. collagen, gelatin, hyaluronic acid, chitosan, alginate, cellulose) and synthetic origins (e.g. polycaprolactone (PCL), polylactic acid (PLA), poly(lactic-co-glycolic acid) (PLGA)), are extensively used for the fabrication of scaffolds due to their ease of processing, chemical versatility, tunable degradability and, in the case of some natural polymers, their resemblance to extracellular matrix (ECM) components [7,8].

Regarding scaffold fabrication, several techniques have been proposed including electrospinning, impregnation and sintering, melt molding, solvent casting, particulate leaching, gas foaming and freeze-drying, or usually combinations thereof. However, most of these techniques show limitations, particularly related to the generation of a controlled porosity with the desired pore size and enough pore interconnectivity to promote cell proliferation, differentiation and growth. It is thus important to understand the various fabrication approaches that have been implemented to control the above mentioned parameters, toward achieving scaffolds with well-organized microstructures. Examples of fabrication strategies with porosity control are inverse opals, which are obtained from colloidal templates to obtain ordered porous structures, ice-templating using frozen ice as the interconnecting porogen, emulsion templating or foaming using supercritical fluids technology. Recently, 3D printing has also emerged as an appealing alternative to the fabrication of 3D scaffolds with sophisticated architectures. For the sake of brevity, we left 3D printing out from this review, details about this fabrication technique can be found in dedicated works [9–12]. We thus focused on highlighting recent advances in the fabrication of hierarchical porous 3D scaffolds and their applications in tissue engineering. We discuss the state of the art of different fabrication approaches to achieve scaffolds with controlled microstructure, along with their associated challenges. We finally propose future directions and perspectives for further research on 3D porous scaffolds for cell culture, toward a better understanding of tissue growth and dynamics, as well as for the development of *in vitro* disease models and drug screening of new therapeutics.

2. REQUISITES FOR SCAFFOLD DEVELOPMENT

Synthetic scaffolds not only work as templates for the cultured cells, but are also required to provide the necessary stimuli to ensure cell survival, close cell-cell

interaction, and further cell differentiation to obtain the desired organ [13]. The ideal conditions for tissue engineering depend on the type of cells and the conditions needed to recreate the microenvironment and induce cell differentiation [14]. Notwithstanding, the basic properties for any scaffold to be suitable for biomedical applications can be summarized into porosity, mechanical properties, biocompatibility and bioresorbability [15], which we briefly introduce below.

Porosity: The structure of the scaffold must ensure that cells can circulate through it, which makes it necessary to create a highly interconnected inner network (over 70% of the total volume) of adjacent pores, with large enough diameters to allow cell diffusion and flow of extracellular matrix (ECM) components [15]. Porous scaffolds can contain pores of different diameters, ranging from several nanometers up to tens of microns, each pore size range being able to promote specific interactions to modulate cell behavior [16]. Depending on the pore diameter, empty cavities can be classified as macro-, micro- and nanopores. Macropores are cavities with diameters larger than 100 μm, used as the niches in which cells are able to group altogether, promoting cell-cell and cell-matrix interactions. These cavities ought to have a high pore volume, not only to provide space for the growing tissue but also to allow for the diffusion of oxygen and nutrients during tissue growth [17]. Micropores (ranging from 0.3 to 100 μm) are normally used as windows between macropores to enhance permeability and support cell diffusion by capillary forces [16]. Finally, nanopores (< 300 nm) can interact directly with cells, thereby promoting cell adhesion by increasing the available surface area [16].

Biocompatibility: The biocompatibility of a scaffold can be defined as its ability to support cell activity by means of molecular signaling, while avoiding any toxic effect on the growing tissue [18]. The main factors involved in these mechanisms include the chemical composition of the synthetic structure, along with the presence of other types of functional biomolecules [19]. Regarding chemical composition, porous scaffolds can be classified into inorganic, such as metals, ceramics or glass ceramics, and organic materials like polymers and composites [20]. Additionally, the biocompatibility of the porous matrix can be enhanced by the addition of biomolecules such as growth factors, either to the bulk matrix or by attaching them to the pore walls to promote direct interactions with the cells [19]. Apart from the chemical composition, other factors such

as the morphology, roughness and rigidity of the pores can also influence cell adhesion and biocompatibility of the porous matrix [20,21].

Mechanical properties: 3D scaffolds should be able to withstand the pressure exerted by the tissue during its development. It is important to maintain the shape and mechanical properties of the interconnected network, as small variations in the pore matrix can influence the biological activity of the cells [17]. Nonetheless, one of the disadvantages of using porous scaffolds is the partial reduction of mechanical strength due to the loss of bulk volume, being replaced by empty cavities and thus increasing the complexity of the system. In addition to providing mechanical support, the scaffold characteristics should also match the mechanical properties of the tissue to mimic the conditions responsible for differentiation stages during tissue formation [22]. As an example, bone tissue engineering is expected to recreate different types of bone structures by varying the compressive strength and Young modulus of the synthetic network [23].

Bioresorbability: During development, the tissue grows to occupy the whole volume of the interconnected porosity. At this point, vascularization is hindered and can lead to a deficit of nutrients and oxygen into the tissue, ending in cell death and tissue malfunction [24]. For this reason, the degradation rate of the scaffold should be proportional to tissue ingrowth, until the whole support is resorbed once it has accomplished its function as a template [18,25].

3. SCAFFOLD FABRICATION

Despite much progress, designing porous scaffolds with well-organized and tailored microstructures for biomedical applications remains a challenge. Special attention is to be paid to the building process to achieve the features required for the targeted application. A number of strategies have been followed to prepare biomaterials with appropriate porosity and interconnectivity. However, most such strategies fail at reproducing a truly ordered and defined microporosity. We review in this section the most important fabrication strategies toward ordered scaffolds with controlled microstructures.

3.1. Inverse Opals

Most of the strategies used to create biocompatible structured materials aim at

mimicking the unique properties of natural biological systems [26]. As an example, natural opals contain 3D crystalline micropatterns composed of silica spheres with diameters ranging from 150 to 300 nm [27]. Such organized structures form within natural systems, such as opal gemstones or butterfly wings, and can manipulate the transmission of incident light, opening up potential applications such as optical switching or photocatalysis [28,29]. These systems are also known as photonic crystals (PhC) for their ability to manipulate the propagation of light by diffraction effects [30]. Synthetic opals have been fabricated by different methods, including the self-assembly of monodisperse colloidal particles. The optical properties of such artificial opals can be tuned by tailoring different parameters, such as the size of the colloidal particles, their chemical composition (and refractive index), and the lattice constant defined by the spatial distribution of the spheres [30,31]. Inspired by photonic crystals, the idea of ordered assemblies has been translated to the fabrication of 3D biomaterials based on the negative replica of a solid template made of colloidal particles [32]. The acquired porous negative lattices thus become porous matrices with well-defined porosity and interconnectivity. They are known as inverse opals (IO) and can be used in a wide range of applications according to the degree of order and the dimensions of their inner cavities [33,34]. In comparison with other pore-inducing strategies such as salt-leaching or gas foaming [4], the main advantage of these materials is their high homogeneity determined by the monodispersity of the particle building blocks, which promotes similar cell-matrix and cell-cell interactions within the whole volume of the scaffold. In this context, inverse opals can be constructed from different materials, ranging from malleable common polymers to solid inorganic oxides [35]. Regardless of the material used for the colloidal template, IOs aimed for tissue engineering purposes are required to contain pores with diameters in the micrometer scale, as cells have average sizes around 20 μm, depending on cell type [33].

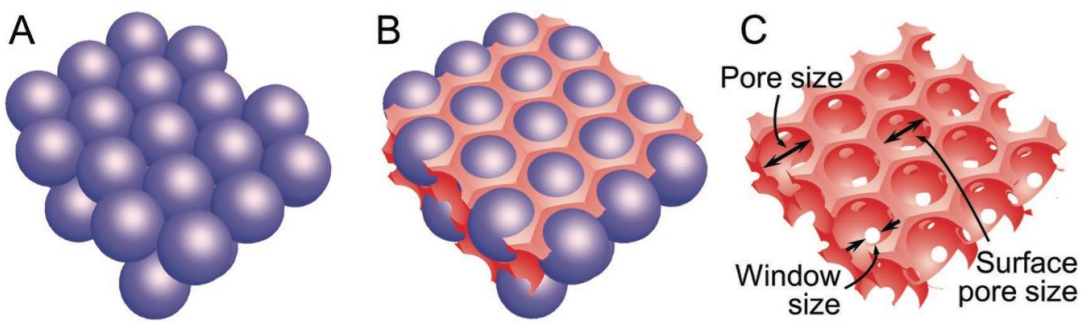

Figure 1. Schematic representation of the main steps through the fabrication of an inverse opal: A) Colloidal assembly and thermal annealing. B) Infiltration of a sol-gel or polymer precursor into the cavities of the ordered assembly. C) Hardening of the inverse crystal (by crosslinking, sintering or freeze drying) and removal of the colloidal template. Copyright (2017) Wiley. Used with permission from ref. 33 (Zhang et al. Inverse Opal Scaffolds and Their Biomedical Applications. Adv Mater 2017;29:1701115).

The synthesis of inverse opals can be summarized into 3 main steps: building an ordered colloidal assembly, infiltration of a precursor sol-gel solution through the template and subsequent solidification and removal of the sacrificial template (**Figure 1**). For the first step, monodisperse colloidal particles are required so they can be arranged into ordered multilayer arrays. The chemical nature of the beads can range from polymer beads, such as of polystyrene (PS) or polymethylmethacrylate (PMMA), to inorganic particles like silica [25]. For the colloidal assembly, several methods can accelerate the process while yielding high quality ordered structures [36]. It is worth noting that, despite simple strategies such as sedimentation can lead to organization of the particles by self-assembly, the process may be assisted or improved by applying external forces. Shaking or sonication can often help displace non-ordered particles into available empty cavities in each layer of the assembly [36].

Once the colloidal particles have been organized, the colloidal crystal is thermally annealed to create connections between adjacent particles, thereby stabilizing the assembly and building necks that act as templates for channels between pores in the resulting inverse crystal. Parameters such as the diameter of the colloidal particles, annealing time and temperature will determine the dimensions of the obtained channels. In a detailed study it was concluded that, although longer annealing times resulted in an increase of channel size, temperature proved to have a major effect, so that even small variations result in channels with significantly different width [34]. The next step includes the infiltration of a precursor through the empty gaps within the annealed template. This process essentially comprises soaking the consolidated template with the precursor solution until the voids get fully covered. In order to accelerate infiltration, external forces such as centrifugation or pressure are typically used [37]. Nonetheless, some conditions such as viscosity of the precursor solution and the size of the available empty spaces in the assembly must be taken into consideration to ensure complete infiltration of the precursor solution. For example, solvents with high viscosity will be hard to force their path into the template, which can be fixed by simple dilution [38].

However, in exchange to reducing the precursor concentration into a bigger volume, it will also be necessary to repeat the infiltration step several times to ensure that all empty cavities are filled up with the organic/inorganic material [38].

The final step comprises the solidification of the infiltrated solution and removal of the colloidal template. IOs composed of either organic or inorganic materials are required to retain their shape and structure upon removal of the sacrificial template. Precursor solutions composed of polymer can be either cross-linked or freeze dried, whereas inorganic IOs are usually obtained through sintering [33]. The methods employed to remove the ordered sacrificial template are dictated by the chemical composition of the colloidal particles. Polymer-based assemblies can be removed either by chemical etching or calcination, while inorganic templates such as silicates require a chemical treatment [39]. It is important to mention that both strategies may affect the stability and porosity of the obtained inverse colloidal crystal. It has been proposed that removal of a polymer template by calcination has a huge impact on the final sizes of the pores, as the template is likely to shrink [39]. This reduction in size also lowers the stability of the hardened-to-be colloidal crystal as it loses its physical support. Thereby, pores can reshape and non-desired cracks may form.

3.2. Emulsion Templating

High internal phase emulsions (HIPEs) are those emulsions in which droplets (internal phase) occupy at least 74% of the total emulsion volume, being the minimum volumetric space required to ensure contact between adjacent droplets [40]. Emulsions are obtained by the mixture of two immiscible phases, known as the continuous phase and the internal or dispersed phase. The dispersed phase usually contains water and constitutes the interconnected network of droplets [41]. On the other hand, the continuous phase is to become the “skeleton” of the 3D matrix and its composition commonly consists of hydrophobic solvents (oils) mixed with monomers, surfactants and a photo-initiator. These systems result in droplets with sizes ranging from few to several hundred micrometers, depending on the synthesis procedure and the composition of each phase [40]. After curing and drying, 3D complex porous morphologies are obtained, containing spherical cavities that originated from droplets, which we refer to as pores, while interconnected channels are termed windows. The tailored dimensionality and interconnectivity of the formed emulsion render these

materials suitable templates for porous scaffolds in 3D cell culture and tissue engineering. In addition to the porosity obtained through emulsification, further levels of porosity can also be defined by varying the degree of cross-linking of the resulting polymer. In tissue engineering, variations in cross-linking also induce changes in the viscosity of the polymeric network, thus promoting retardation in cell diffusion [42].

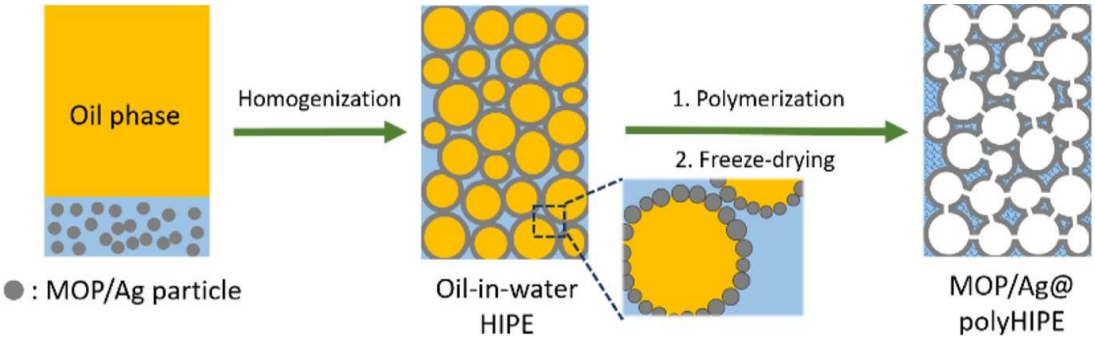

Figure 2. Schematic representation of the preparation of HIPE with silver-incorporated melamine-based microporous organic polymer (m-MOP/Ag). Adapted with permission from ref. 52. Copyright © 2019 Elsevier.

In the context of tissue engineering, the porous matrix should have pore diameters above 100 μm and windows of at least the diameter of the cells under study, so as to provide an open path for easy cell diffusion [43]. Some of the parameters that are known to play an important role on droplet size and formation of open/closed pores are the volume ratio of the internal phase, the chemical nature of the surfactant and its concentration [44,45]. In order to stabilize droplets with large diameters, polymers such as partially hydrolyzed polyvinyl alcohol (PVA) are commonly used as co-surfactants, due to their amphiphilic nature and biocompatibility. By increasing the molecular weight of the polymers, it is possible to achieve higher droplet stability, within a certain concentration range. However, the same weight increment can also induce a higher viscosity, which would in turn hinder the emulsification step [46].

When referring to the presence of open/closed pores and to the size of the windows, surfactant concentration plays a major role. In a selected piece of work [47], the excessive use of amphiphile was found to cause wall thinning at the contact site between adjacent emulsions. Upon further shrinkage during crosslinking, open windows formed where the emulsion walls were thinnest. This could become a method to obtain open cavities by introducing large surfactant concentrations to replace polymer in the droplet membrane. We should however give a word of caution, as an increase in surfactant concentration can also lead to formation of smaller droplets because of the

concomitant decrease in surface energy per unit area [48]. On the other hand, the presence of surfactants may also affect the behavior of cultured cells by damaging the cytomembrane, even inducing cell death [49]. Alternative techniques have been reported to reduce the required amount of surfactant for pore synthesis, coupled with HIPE. In one such strategy, emulsions can be further stabilized by addition of solid colloidal particles [50]. The system composed by the combination of solid beads with two immiscible phases is known as Pickering emulsion and its improved stability is explained by the irreversible adsorption of the particles at the oil/water interface, which provides enough mechanical hindrance to avoid coalescence and retain the original pore size [51,52]. A schematic representation of HIPE preparation is shown in **Figure 2**. A different strategy to obtain large pores comprises the addition of small amounts of water-miscible organic solvents into the aqueous phase [44]. For example, tetrahydrofuran 1% (v/v) facilitates the transport of water molecules from smaller droplets to larger ones through the continuous phase, thus promoting Ostwald ripening and increasing the diameter of the resulting pores.

In addition to the use of surfactants, a drawback of emulsion templating is the use of significant amounts of organic solvents. Not only they are often environmentally harmful, but also require consideration of viable strategies for subsequent removal, due to potential toxic effects that would hinder the biocompatibility of the porous matrix [53]. In this respect, supercritical carbon dioxide-in-water emulsions can be considered toward solving this problem, as they can generate homogenous droplets while using only CO_2 and water as the dispersion media [53]. Supercritical CO_2 ($scCO_2$) has indeed become of interest for biomedical applications due to its low toxicity and high abundance, as will be described below regarding the preparation of foams from supercritical fluids [54]. Notwithstanding, despite its multiple advantages with respect to other solvents, it also poses drawbacks when related with emulsions due to the low solubility of most polar biomolecules and polymers [55]. Some types of fluorinated polymers and silicon proved to be highly soluble in CO_2, but we still need to find alternative low-cost and easily degradable materials for droplet templating [56].

3.3. Ice templating

As described above, the most common processes to fabricate porous scaffolds involve the use of solvents or templates that are subsequently removed, while ensuring

biocompatibility. In this context, cryogenic processes become an interesting alternative for the preparation of porous scaffolds due to the high biocompatibility of the template (ice crystals) and its easy removal (no chemical reactions, by-products or purification steps) [57,58]. Cryogenic processes are based on freezing aqueous colloidal suspensions (either ceramic, metallic or polymer-based), followed by defrosting [59,60]. When ceramic composites are employed, a purely inorganic material can be obtained upon high temperature calcination of the composite scaffold to remove the organic phase [61]. During the freezing process, ice crystallization segregates the solutes dispersed in the aqueous phase from the ice phase, resulting in structures characterized by "walls" or "fences" of matter enclosing ice crystals (**Figure 3**) [57,62]. Subsequent drying, involving simple thawing or freeze-drying, results in cryogels that contain macropores corresponding to the empty areas left by the ice crystals. Thus, the microstructure of the scaffold is a negative replica of ice before drying [63]. It is worth noting that the use of freeze-drying instead of simple thawing avoids drying stresses and shrinkage, which usually lead to crack formation and warping [59].

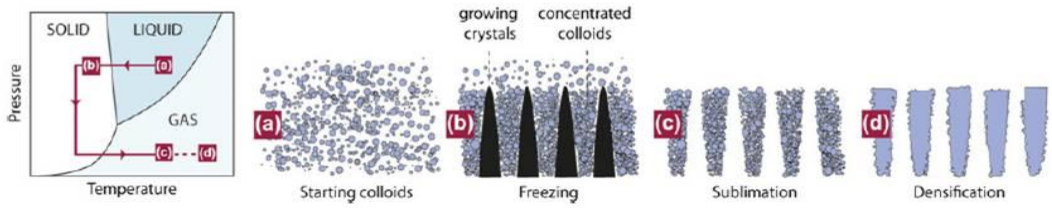

Figure 3. Schematic representation of the ice-templating fabrication process. Reprinted with permission from ref. 66 © Copyright: © Materials Research Society 2013.

The morphology of the macroporous structure can be further tuned by controlling the freezing conditions, such as temperature or the direction of sample immersion into the cryogenic fluid. Lamellar thickness, inter-lamellar spacing, bridge density or surface roughness can thus be tailored to achieve the desired microstructure [64]. By controlling the growth direction of ice crystals, materials with a preferential porosity orientation and highly sophisticated structures can be prepared [59,65,66]. Therefore, unidirectional freezing can be employed for the production of different types of morphologies. Tamon et al. were arguably the first to use unidirectional freezing with silica gels, for the preparation of honeycomb-like scaffolds after the pseudosteady state growth of ice crystals [67,68]. A different method was used for the directional freezing of ceramic slurries using polytetrafluoroethylene molds placed between two copper cold fingers [63], typically resulting in scaffolds with open interconnected macropores, ranging from

20 to 100 µm in their smallest dimension and 50 to 500 µm in the largest one. Interestingly, the speed of the solidification front can be tuned through the temperature of the cold fingers, thereby defining the size of the obtained ice crystals. Using this procedure, materials with three distinct porous zones were obtained (**Figure 4**), depending on the distance to the cold finger, with varying porosity. The formation of heterogeneous pores along the scaffold can be prevented by continuous immersion into liquid nitrogen at a constant rate [62]. The ice front is thereby maintained at a constant distance from the nitrogen level during immersion, leading to homogeneous porous structures [69].

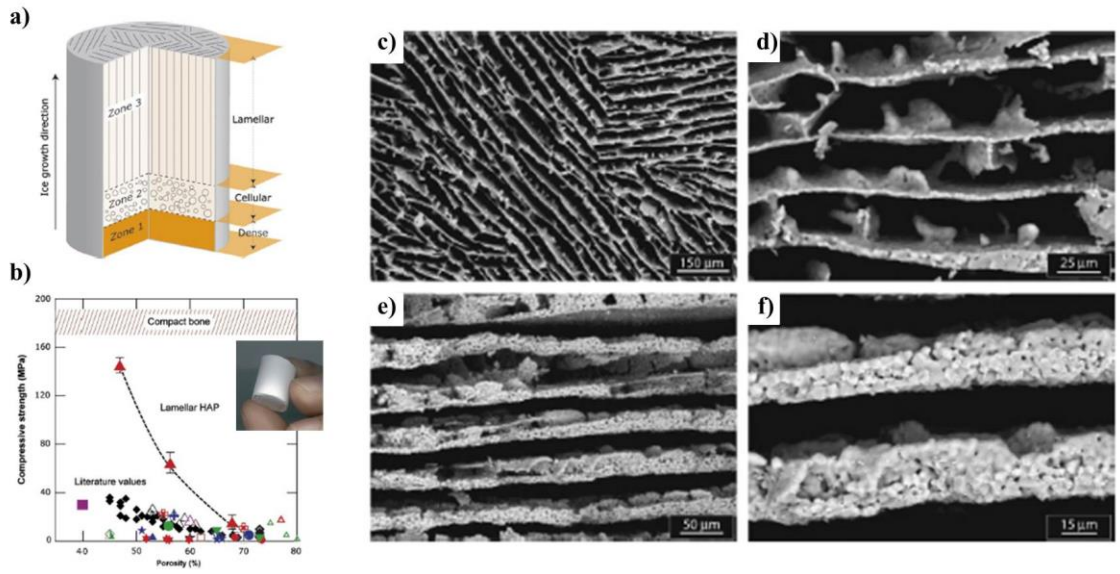

Figure 4. (a) Structure of an ice-templated sample featuring three distinct zones with pore dimensions depending on the processing conditions. (b) Maximum compressive strength achieved by freeze-casting at a cooling rate of 5 °C/min vs. porosity, including the comparison of porous hydroxyapatite scaffolds with compact bone and literature values. (c-f) SEM images of porous hydroxyapatite scaffolds with 64% porosity (cross-section parallel to the ice front (c,d) and section perpendicular to the ice front (e, f)). Adapted with permission from ref. 59. Copyright © 2006 Elsevier.

Del Monte et al. introduced the term "ice segregation induced self-assembly" (ISISA), to describe this unidirectional freezing bottom-up approach and employed this technique to aqueous gels made of colloidal silica, PVA solutions, PEG-based hydrogels or chitosan/multi-walled carbon nanotubes (MWCNT) and chitosan/carbon nanofibers (CNF) composites (Figure 5) [57,58,70–75]. The authors additionally demonstrated that ISISA is a versatile and biocompatible technique allowing the incorporation of enzymes or liposomes into the hierarchical materials [70,76]. Another major advantage of unidirectional freezing is that it offers the possibility to encapsulate

living cells within the 3D scaffolds [77]. Scaffolds with pore sizes ranging from 25 to 90 μm and 85% porosity were achieved by varying the freezing rate.

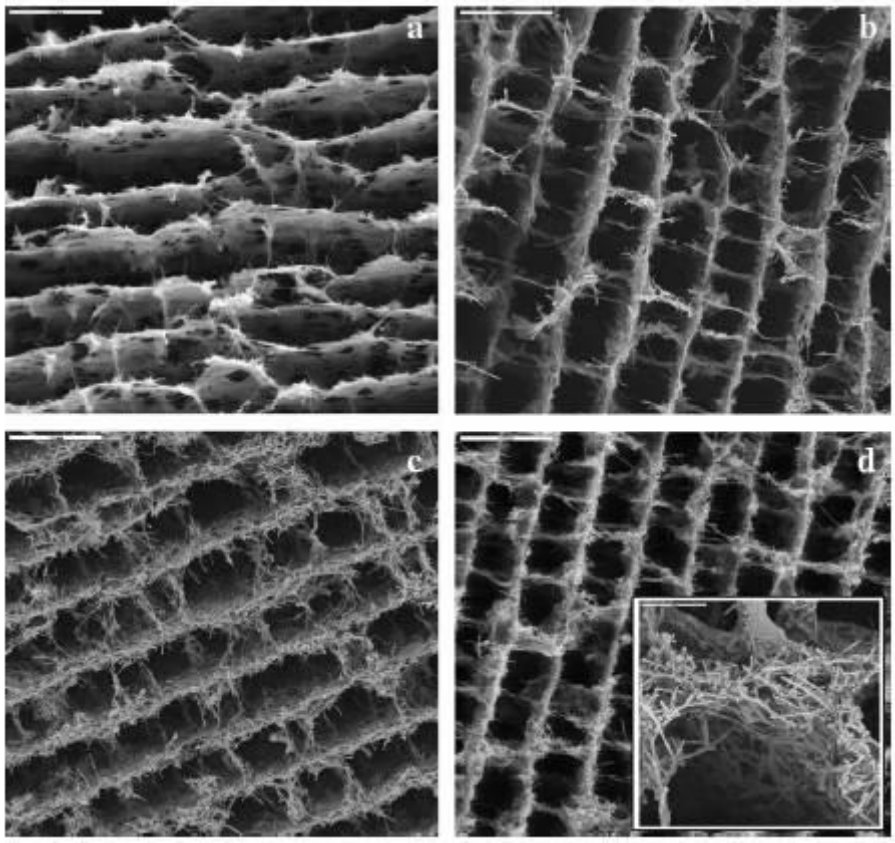

Figure 5. SEM micrographs of cross-sectioned MWCNT/chitosan scaffolds with different MWCNT concentrations: 66 wt% (a), 80 wt% (b) and 89 wt% (d). Scale bars = 20 μm. The inset shows interconnected MWCNTs forming the walls of the scaffold (scale bar is 5 μm). Reprinted with permission from ref. 71 (J. Phys. Chem. C 2007, 111, 15, 5557–5560) Copyright (2007) American Chemical Society.

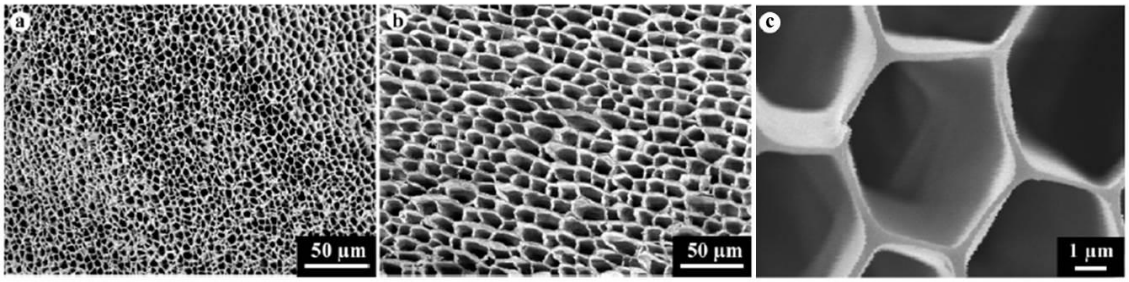

Figure 6. SEM images of the cross-sections of silica gel microhoneycombs with different macropore sizes, prepared at 77 K using different immersion rates of 20 cm/h (a), 6 cm/h (b). (c) High magnification image of the microhoneycombs. Adapted with permission from ref. 78, (Chem. Mater. 2005, 17, 3, 683–689) Copyright (2005) American Chemical Society.

The chemical composition of ice-templated scaffolds can also be tailored to achieve different microstructures. Aging of the gelling solution is critical, as soft hydrogels result in microhoneycombs, whereas firmer hydrogels form fibers with polygonal cross-sections (Figure 6) [78]. Additionally, slurry concentration and particle size also affect the porosity thickness/layer thickness and the pore morphology [64]. Metallic nanoparticles, such as gold nanoparticles, are also compatible with ISISA and their incorporation has been shown to affect the microporous morphology of the scaffolds [69]. The viscosity of the solution or the gel strength of polymer-based hydrogels also affect the microporous structure, varying from lamellar-type to cellular-type morphologies, as the strength of the network increases. It has been observed that, when using polymers, their molecular weight influences the size of the crystals and smaller ice crystals are observed as the molecular weight increases. Ice-templating can also enhance the mechanical properties of scaffolds made of colloidal particles in the presence of polymers and crosslinkers [79]. In this approach, cross-linking takes place in the frozen state, where the exclusion from growing ice consolidates particles and polymer into the walls of the scaffold, yielding elastic composite scaffolds due to the formation of connections by the cross-linked polymeric mesh.

3.4. Supercritical Fluids (SCFs)

Gas foaming of polymers or composites using supercritical fluids (SCFs), such as supercritical CO_2 ($scCO_2$) or nitrogen, can be used to fabricate 3D porous scaffolds with controlled pore structure, with no need for harmful organic solvents, incompatible with cells and biological tissues [80]. For the same reason, the working conditions during foaming with SCFs are compatible with the incorporation of biomolecules such as growth factors or antibacterial agents [81–83]. Therefore, the use of supercritical fluids represents a green, low cost alternative for scaffold fabrication.

When working with $scCO_2$ for polymer processing, pressure and temperature are maintained above the critical point of CO_2 (T_c = 31.1 °C, P_c = 73.8 bar) to saturate the polymer with $scCO_2$, thereby reducing the apparent glass transition temperature or melting point of the polymer to its processing temperature [84]. During quenching by depressurizing or increasing temperature, thermodynamic instability results in supersaturation of dissolved CO_2 in the polymeric matrix and pore nucleation takes place, with pores growing until the polymer vitrifies or the matrix viscosity is increased.

Several parameters such as pressure, temperature, supercritical fluid composition and depressurization profile play a key role in defining the porosity and pore size distribution of the scaffolds (**Table 1**, **Figure 7**) [81,84–86]. When dealing with semi-crystalline polymers, CO_2 sorption facilitates chain mobility and the rearrangement of polymer chains becomes easier, usually reducing the crystallization temperature [87]. The melting temperature is also likely affected because polymer swelling induces a tendency of the chains to rearrange into more extended configurations, disturbing the crystalline structure. To increase the solubility of crystalline polymers, organic solvents can be incorporated to the mixture [88], which can also be combined with other strategies, such as thermally induced phase separation, for the preparation of porous scaffolds [89–91]. The main weakness of this technique is the reduced pore interconnectivity, which can again be increased by addition of compatible organic solvents, micro or nanoparticles, or plasticizers [81,92,93]. Another disadvantage of foaming using SCFs, which is particularly relevant for the use of these materials as cell culture scaffolds, is the formation of a dense nonporous skin attributed to the rapid diffusion of the fluid out of the edges of the sample [87]. This issue can be solved by mechanical removal of such a skin, after scaffold formation. Bhamidipati et al. and Reverchon et al. nicely reviewed the use of carbon dioxide for the preparation of 3D porous scaffolds, following different processing options such as CO_2 into gas foaming, SCF-assisted phase separation or SCFs emulsion templating [94,95]. Even if interesting materials result from the application of these approaches, we focus on scaffolds produced by foaming with SCFs to achieve a more homogeneous and well organized porosity. In an early study of the use of SCF foaming toward porous scaffolds for tissue engineering [96], poly(D,L-lactic-co-glycolic acid) (PLGA) was the polymer of choice and porous scaffolds were obtained with pore sizes around 100 μm and porosities up to 93%, using CO_2 at 5.5 MPa and room temperature. In a subsequent work by the same authors, NaCl particles were incorporated into the formulation to increase the porosity and interconnectivity of the scaffolds [96]. The successful adhesion and proliferation of smooth muscle cells within the scaffolds revealed their potential for tissue engineering.

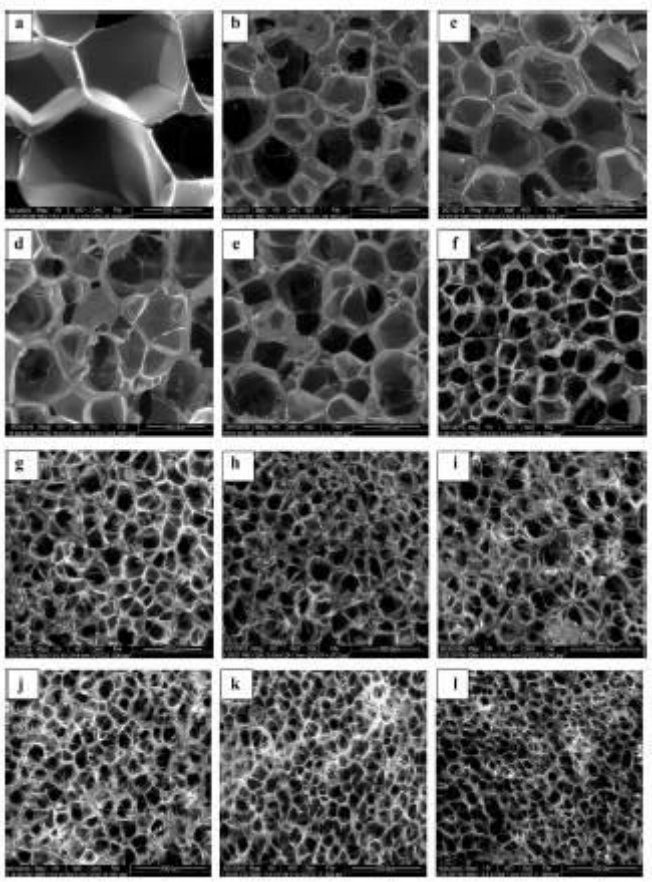

Figure 7. Environmental SEM micrographs of PLGA/HAp/Collagen scaffolds prepared at different saturation pressures. Scaffolds were prepared at 40 °C for 45 min at: a) 8 MPa, b) 10 MPa, c) 12 MPa, d) 14 MPa, e) 16 MPa, f) 18 MPa, g) 20 MPa, h) 22 MPa, i) 24 MPa, j) 26 MPa, k) 28 MPa, and l) 30 MPa. Reprinted with permission from reperence 86. Copyright © 2011 Elsevier.

Table 1. Processing conditions and resulting pore size and porosity of scaffolds prepared via SCFs technology.

Scaffold Composition	Blowing Agent	Foaming T (°C)	Saturation Pressure (MPa)	Soaking time (h)	Depressurization (MPa/min)	Pore Size (μm)	Porosity (%)	Ref.
PCL	CO_2	37	10	0.5	1.5	50-200	62	82
	CO_2	40	20	1	4	87-525	60-75	97
	CO_2	30-40	10-20	-	0.1-2	110-1500	-	85
	CO_2/ethanol	35-45	12.3-20.5	-	-	50-80	-	86
	CO_2	30-40	10-18	-	0.1-2	150-340	40-70	83
	CO_2/organic solvent	50	20	1	Two step venting/foaming	50-1500	-	91
				17		400-700		

PCL/TZ PCL/TZ/HA	CO_2	44	150	-	4200	40	47.5	80
		80					35.3	
		100				200	39.5	
PCL PCL-Eugenol	CO_2	45	20	17	Two step non-isothermal	500-700	82-84	81
					Vessel venting	500-700	82-84	
					Single non-isothermal	80	74	
PCL PCL-HA	CO_2	40	20	1-17	Two step depressurization	50	65-70	84
		45				100	80	
	CO_2/EL	40				100-200	80-85	
		45				100-50 200-400		
	CO_2/EA	40				<100 200	70	
		45				100 200-300	80	
PCL/silica	CO_2	160	16	2	-	40-930	50-60	92
PLGA	CO_2	-	5.51	48	-	190-440	85-97	95
		30-35	25	1	-	250	81	121
PLGA/HA/Collagen	CO_2	35-60	8-30	1.5	-	97-730	48-92	115
PLA	CO_2/EL	35	20	1.5	Fast (30 s) or Slow (360 s)	50-500	-	96
		40				25-150		
	CO_2/acetone	60-80	14-61	-	-	5-400	-	87
PDLLA	CO_2	35	20	0.5	0.5	200-400	56-67	118
			17.32	-	-	250	70	120

			23.2	-	2.32	10-1200	-	116
					0.77	10-1000		
					0.52	10-800		
					0.39	10-600		
CS	CO_2	37	6-16	-	1	30-40	-	98
Elastin	CO_2	37	3-15	0.5	-	14-5	-	99,102
		37	0.1-6			20-80		
Chitin	CO_2	80	6.5-12.5	3	-	60-160	-	100
Gelatin Gelatin/CS	CO_2	26	5-8-11	2	-	300-25-22	-	101
		40	100			50		

Salerno et al. extensively applied the SCF technology to porous scaffolds using typical polymers for biomedical applications, such as polylactic acid (PLA) or polycaprolactone (PCL) [80,81,84,97,98]. Biodegradable PCL-based scaffolds were prepared via supercritical CO_2 foaming, in combination with thermoplastic zein (TZ) and hydroxyapatite (HAp) particles [80]. By modulating composition and foaming temperature (T_F), the porosity of the scaffolds could be controlled. If foaming takes place at a T_F above the melting temperature, pores nucleating in the PCL phase coalesce before crystallization of the polymer matrix and bigger pores are formed. At even higher temperature, larger pores (200 μm) grow due to a lower stiffness of the matrix. To preserve heat-labile molecules, supercritical CO_2 foaming can be also performed at low temperature, known as "solid-state foaming" [97]. However, this approach becomes more difficult in the case of semi-crystalline polymers, where the highly ordered structure reduces the diffusion of $scCO_2$ and polymer plasticization. Therefore, the resulting scaffolds show inhomogeneous pore structures and low porosity. This is the case of PLA, an interesting choice toward biodegradable scaffolds, also affected by

CO_2-induced crystallization during the sorption stage. To circumvent these problems, solid-state foaming of PLA can be performed in the presence of ethyl lactate, resulting in scaffolds with homogeneous morphology and pore sizes ranging from 50 to 500 μm (**Figure 7**) [97].

When using hydrophilic polymers, such as hydrogels, pore formation takes place by dissolving CO_2 in the aqueous phase [99]. Hydrogel foaming can be applied to either water-insoluble polymers such as chitin or elastin, which form swollen dispersions in aqueous solution, or to water-soluble polymers such as chitosan or gelatin, being also compatible with the incorporation of cross-linkers such as glutaraldehyde or genipin [99–103]. It is worth noting that the drying step after foaming is critical to maintain the porous structure. Air-drying can produce extensive shrinking and collapse of the porous structure, thus mild freeze-drying is generally the technique of choice to produce stable porous materials [102]. The increase in processing pressure leads to a reduction in pore size, which also depends on hydrogel composition, cross-linking degree and processing temperature [100,103]. This processing technique reduces also the pore wall thickness, as compared to conventional hydrogels, and creates channels through the 3D structure [100]. Another advantage is that this type of foaming avoids the formation of a skin layer, commonly observed in hydrogel processed by traditional methods [99].

4. POROUS SCAFFOLDS FOR TISSUE ENGINEERING

3D scaffolds with hierarchical porous structures have received considerable attention in the biomedical field, with a special focus on tissue engineering applications. As mentioned in the previous section, certain requirements are to be fulfilled by the scaffolds, to support tissue growth and regeneration. The fabrication techniques discussed in this review open the way toward the design of porous scaffolds with tailored features to support the target tissue. **Table 2** summarizes the main characteristics of scaffolds produced by different processing routes, as well as the main advantages and disadvantages to be faced in each case. This section highlights the most recurrent tissues engineered on the basis of well-organized porous scaffolds.

Table 2. Characteristics, main advantages and drawbacks of 3D scaffolds produced by different fabrication techniques.

Fabrication Technique	Pore size (μm)	Interconnectivity	Reproducibility	Advantages	Drawbacks	Applications in TE
Inverse	0.01 –	Tunable by	High	• High level of organization	• Need for materials	Bone TE

Opals	200	thermal annealing (High)		• Homogeneous porosity • Tunable interconnectivity • Diversity in chemical composition • Possible post-functionalization to enhance biocompatibility	with enough mechanical strength • Full infiltration of precursor solution to avoid scaffold collapse • Removal of the colloidal assembly may damage scaffold structure	[33,106- 108] Cardiac TE [137-140] Neural cell growth [25,124-128]
Emulsion Templating	0.1-100	Tunable by chemical composition (Poor to high)	Poor/Medium	• Heterogeneous porosity (similar to natural tissue morphology) • Possibility to couple with colloidal particles for controlled porosity • Diversity in chemical composition • Fast	• Hard to obtain pore/channel size homogeneity • Low reproducibility • Need for organic solvents • Need for co-surfactants to open porosity	Bone TE [109, 110] Neural cell growth [42, 129, 130]
Ice Templating	10-500	High	High	• Wide variety of materials • Biocompatible • Easy template removal • Incorporation of enzymes, liposomes, living cells • Tailored microstructure (honeycomb, lamellar, cellular) • Good mechanical properties • Gradient porosity	• Cell proliferation limited to few layers • Limited sample size • Long processing time for big samples	Bone TE [63,111-114] Neural Cell growth [131-133]
SFCs	50-500	Reduced/Poor	Medium	• Avoids harmful organic solvents • Compatible with biomolecule incorporation (growth factors, antibacterial agents) • Low cost • Good mechanical properties	• Formation of dense nonporous skin • Limited pore interconnectivity • CO_2 solubility in the foaming phase limits application	Bone TE [80,81,115-122]

4.1. Bone tissue engineering

In tissue regeneration, the cells involved in organ repair must reach the damaged region, so as to create an extracellular matrix that induces the formation of replacement tissue [104]. The healing process can be supported by porous scaffolds that facilitate cell adhesion and growth, while allowing the diffusion of oxygen and nutrients to the adhered cells [105]. In order to mimic the same environment as that in real bone, the scaffold ought to feature optimal porosity for osteoblasts to properly diffuse, and contain osteogenic factors to promote bone repair [106]. The supporting scaffold is

usually loaded with derivatives from the apatite family, which are known to induce cell differentiation in biological tissue [107]. We review in this section the use of various scaffolds introduced above.

Colloidal inverse opals are appealing for tissue regeneration because their physicochemical properties can be readily controlled [108]. One of the main advantages is the possibility to tailor the surface of the inner cavities by either preparation of sol-gel composites and/or post-functionalization [33]. Although both strategies can promote cell differentiation when growth factors are included, it is important to take into consideration that sol-gel processes will determine both the chemical and mechanical properties of the porous construct, whereas post-functionalization would mainly change the functional groups on the pore surfaces [107,109]. As an example of the importance of cell-differentiation factors, Choi et al. studied the enhanced differentiation of osteocytes at PLGA scaffolds loaded with HAp (Figure 8) [109]. Over a 4-week period, preostoblasts showed a lower proliferation rate in non-coated PLGA scaffolds, as compared to the constant rate observed within a PLGA/HAp porous network. The failure to significantly increase the number of proliferated cells in the coated scaffold was explained by changes in preoteoblasts differentiation, due to interactions of the precursor cells with bone growth factors present in the functionalized porous matrix.

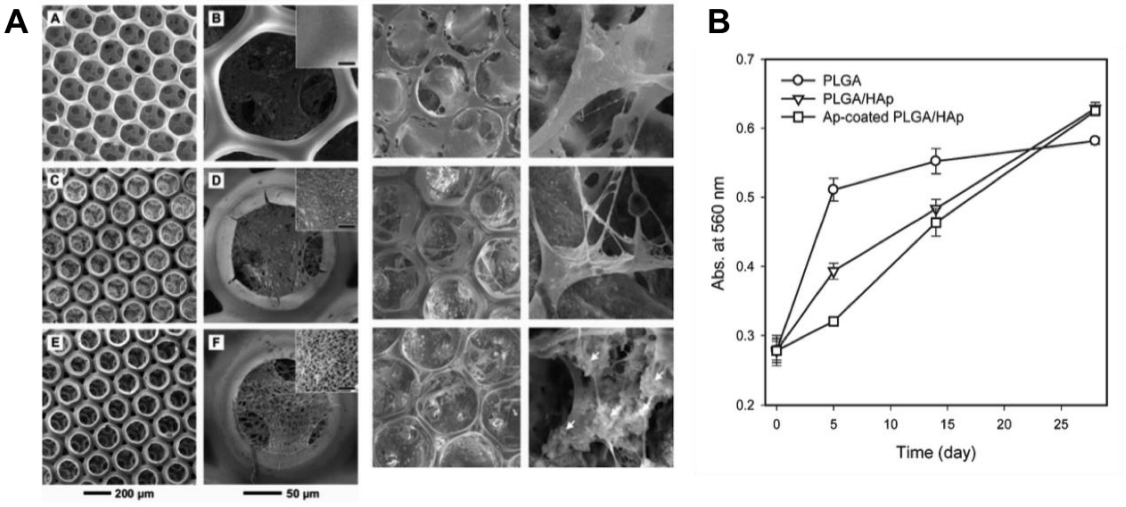

Figure 8. A) SEM images of scaffolds made of: PLGA (A, B), PLGA/HAp (C, D), and HAp-coated (E, F). SEM images on the right-hand side panels show the respective scaffold cultured with preosteoblast cells. B) Proliferation of preosteoblasts cultured on various scaffolds (n = 3). Adapted with permission from ref. 109, Langmuir 2010, 26, 14, 12126–12131. Copyright (2010) American Chemical Society.

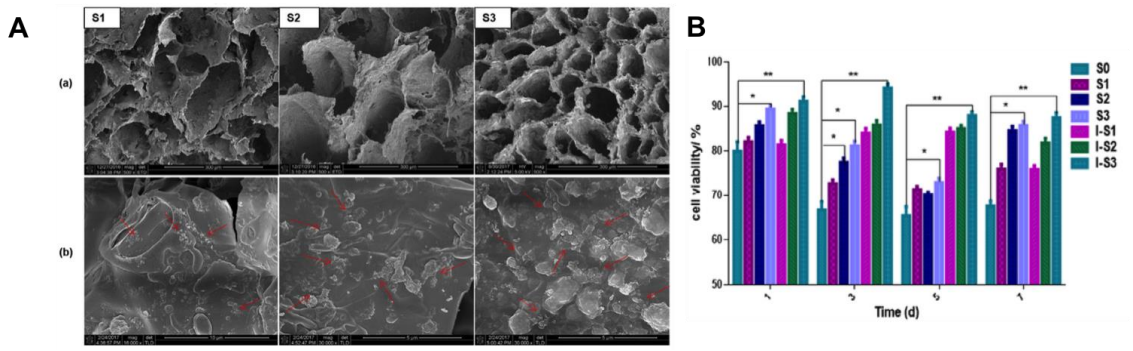

Figure 9. A) SEM images of *in vitro* mineralized HaP/carboxymethyl cellulose/PLGA scaffolds with different wt% of nHAP: S1 (0.75 wt%), S2 (1.5 wt%), S3 (3.0 wt%). The red arrows point toward inorganic apatite crystals. B) Osteoblast proliferation in various scaffolds, by CCK-8 assay. Adapted with permission from ref. 110. © 2020 Elsevier.

On the other hand, HIPE template scaffolds have the advantage of allowing the introduction of precursors within solvents of different polarity. The application of emulsions as templates not only provides control over pore morphology but also allows the addition of water-soluble materials to an inorganic matrix solubilized in the continuous phase [110]. In an interesting example, PLGA hybrid scaffolds were functionalized with nanohydroxyapatite (nHAp), previously mixed within the aqueous phase. After hardening the structure by UV-crosslinking, the growth factors were entrapped into the walls of the voids, ultimately resulting in more extensive cell differentiation than for non-functionalized matrices (**Figure 9**). Pickering emulsions have also been used to synthesize heterogeneous porous scaffolds by mixing PMMA beads with a polymeric emulsion containing droplets smaller than the colloidal beads [111]. Upon self-assembly and annealing of the colloidal particles, the template was impregnated with a HIPE of divinyladipate and cross-linked to acquire a polyester network. Biocompatibility and cell adhesion of human osteoblasts were found to be superior for scaffolds templated by Pickering emulsions than for other HIPE scaffolds. The presence of bigger pores resulting from the removal of colloidal particles was proposed to be responsible for the enhancement of the overall cell viability.

A limiting factor of scaffolds for bone regeneration is still their poor mechanical response associated with their porous nature. Therefore, their applications are often limited to the regeneration of bones submitted to low stress. To circumvent this drawback, stronger porous scaffolds are needed. The ice templating approach can be employed for the preparation of hydroxyapatite-based porous scaffolds with good mechanical properties for bonne tissue engineering [63]. Inspired by nacre, layered

materials have been developed by controlled unidirectional freezing of ceramic suspensions. These porous scaffolds are then filled with a selected second phase (epoxy or metallic) to obtain dense composites. Scaffolds with well-defined pore connectivity and open porosity to allow bone ingrowth were achieved. The resulting scaffolds showed mechanical properties similar to those of bone, despite their high porosity. Following the ISISA approach, del Monte and co-workers prepared MWCNT/chitosan scaffolds with high MWCNT loadings (up to 89 wt.%), featuring a well-defined 3D microchannel porous structure for supported cell growth [112]. Efficient cell growth and proliferation was observed after 4 day cell culture within the scaffolds, both lateral and in depth. However, as also observed for inverse colloidal crystals, cell proliferation within the scaffold is limited to just a few layers of cells since nutrient diffusion deeper inside the material is hindered. The authors studied the evolution of mouse-derived muscle myoblasts (C2C12) to an osteoblastic lineage both *in vitro* and *in vivo* (following implantation of the scaffolds in muscle tissue), in the presence of the recombinant human bone morphogenic protein-2 (rhBMP-2), an osseoinductor protein (**Figure 10**). Bone tissue regeneration was observed after 3 weeks along with scaffold degradation, which was replaced by cells. Following this work, similar scaffolds were prepared by incorporating HAp [113]. The scaffolds were formed by interconnected MWCNT/chitosan sheets arranged in parallel layers crossed by pillars and with homogeneously distributed HAp clusters at the internal surface of the macrostructure. *In vitro* experiments proved the potential of these scaffolds for bone tissue growth upon differentiation of C2C12 cells toward collagen-expressing cells. Similar scaffolds with a pore size range between 20 and 150 μm have also been prepared using doped MWCNTs to study their effect on cell viability of periosteum mesenchymal stem cells [114]. The effect of doped MWCNT was more pronounced for longer times of cell culture and nitrogen-doped MWCNTs were less effective than oxygen-doped ones, indicating that the functionality of MWCNTs was important for their affinity to specific cells.

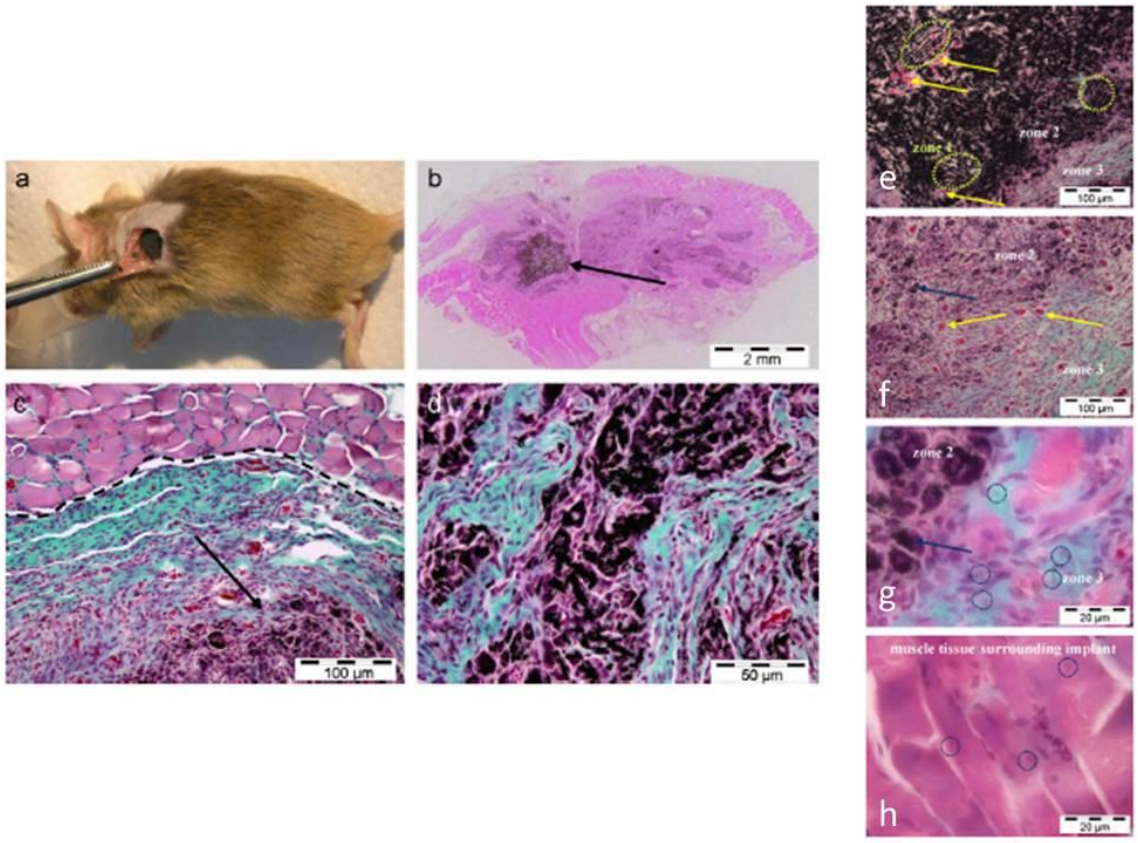

Figure 10. (a) Surgery implantation of rhBMP-2 adsorbed MWCNT/chitosan scaffolds into mouse subcutaneous muscular pocket. (b) Optical micrograph showing regenerated bone tissue and a fraction of MWCNT/chitosan scaffold. (c) Optical micrograph showing a detail of regenerated bone tissue (collagen expressing cells in blue-green, muscle tissue in pink). (d) Optical micrograph showing a detail of remaining scaffold plenty of fibroblasts (purple), prior to its disassembly and colonization by collagen expressing cells (blue-green). (e-g) Optical micrographs showing 3 zones observed after 3 weeks of scaffold implantation with intact scaffold (green circles), non-differentiated fibroblasts (purple cells) and fully disassembled scaffold, respectively. (h) Optical micrograph of few single MWCNT/chitosan dispersed within muscle tissue surrounding the implant. Adapted with permission from ref. 112. Copyright © 2007 Elsevier.

Ice-templating has also been employed for the preparation of HAp scaffolds with gradient channel structures displaying a capillary behavior that favors transport of water and nutrients within the scaffold (**Figure 11**) [115]. To generate the gradient, lamellar ice crystals were grown preferentially from a central copper rod, outward to the plastic mold used during the freezing process. Therefore, an increasing channel width was formed from the center toward the edge of the scaffold. In this case, scaffolds with self-seeding ability when in contact with mesenchymal stem cells (MSCs) were prepared, and spontaneous capillary flow was observed and attributed to the presence of gradient channel structures, showing promising properties for bone tissue-engineering applications.

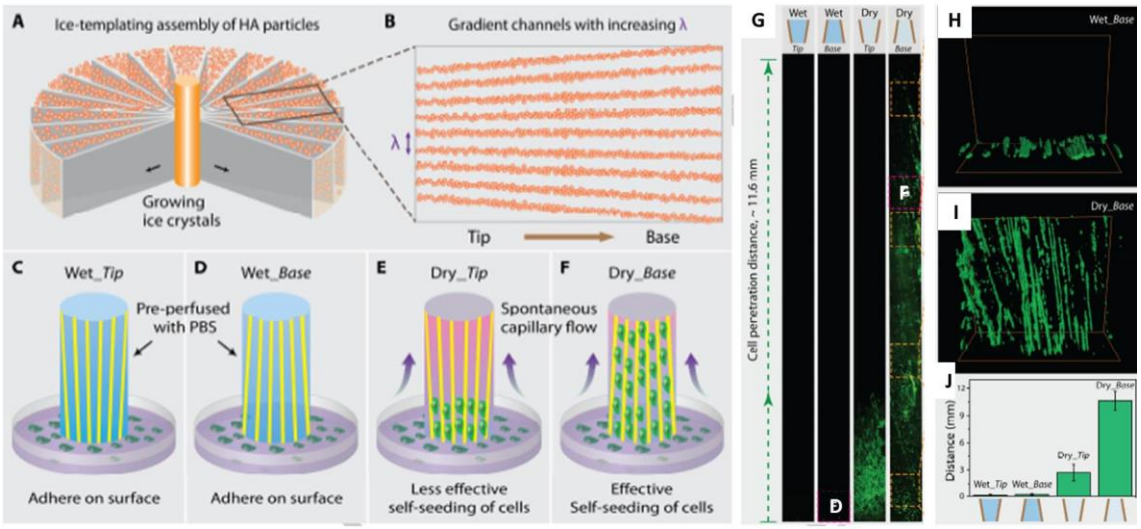

Figure 11. (A,B) Scheme of the fabrication of the gradient ceramic scaffold and cell-seeding experiment. Fabrication of the scaffold where a ceramic slurry is frozen from the cold finger at the center, creating a lamellar structure oriented parallel to the freezing direction. (C-F) Study of the capillary effect of the gradient channels on seeding cells. (G-J) Cell-seeding experiments on wet and dry gradient scaffolds: fluorescent images after seeding cells (G), 3D confocal fluorescent image showing cells for wet base and dry base (H, I), statistical data about the penetration distance of cells (J). Adapted with permission from ref. 115. Copyright © 2015 Elsevier.

Scaffolds processed using SCF technology can also meet the requirements for use in bone tissue engineering applications. For example, PCL-TZ blends have been combined with HAp for the preparation of 3D porous scaffolds for bone repair [80]. Composites processed at a T_F of 100 °C achieved suitable porosity (39.5%), pore size distribution (200 µm), mechanical properties (with elastic compression modulus higher than 10 MPa) and biodegradability for bone tissue engineering. Extraction of TZ resulted in scaffolds with 60% overall porosity and open macropore structure. Biocompatibility studies with osteoblast-like MG63 and human mesenchymal stem cells (hMSCs) showed good cell adhesion and colonization. The incorporation of eugenol to $scCO_2$ increased PCL plasticization, thereby reducing its viscosity and formation of scaffolds with larger pores [81]. By adjusting the depressurization profiles, scaffolds with up to 84% porosity and mean pore size of 530 µm were obtained. Incorporation of eugenol also improved pore interconnectivity and water permeability in the scaffolds. Interestingly, *in ovo* CAM assays confirmed the ability of the scaffolds to promote cell and tissue growth. Moreover, the antimicrobial activity of eugenol could prevent bacteria adhesion after implantation.

An alternative formulation of scaffolds with PLGA/collagen/Hap was also prepared under supercritical conditions [86]. The authors studied the effect of saturation temperature, pressure and saturation time on the properties of the scaffold to achieve large pore sizes, ranging from 100 to 500 μm. These results revealed that this polymer composition is more sensitive to the processing conditions than other polymers, such as PCL. Cell growth studies confirmed osteoblast cell attachment and proliferation, as well as cell infiltration and migration deep into the 3D network (**Figure 12**). The depressurization rate and the molecular weight of the polymer can also affect the properties of PLA-based scaffolds [116]. Rapid depressurization resulted in scaffolds with homogeneous pore distributions, whereas a lower depressurization rate leads to a wider pore size distribution and more interconnected pores. Regarding the mechanical properties, an increased depressurization rate produces scaffolds with larger Young's modulus due to the increased relative density of the scaffolds. PLA-based scaffolds foamed by supercritical fluids showed mechanical properties similar to bone when high molecular weight (57 kDa) PLA was used [116].

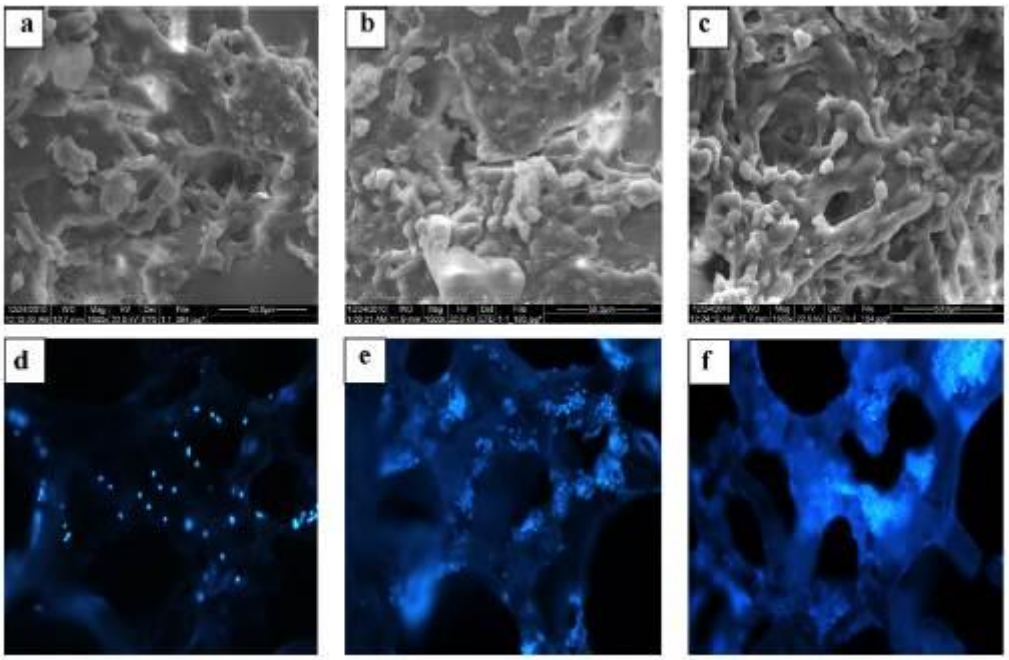

Figure 12. Environmental SEM micrographs and confocal scanning laser microscopy photographs of cell-seeded PLGA-Collagen-HAp scaffold after culture for 3 days (a,d), 7 days (b,e), and 14 days (c,f). Reprinted with permission from ref. 86. Copyright © 2011 Elsevier.

3D porous scaffolds can be employed to simultaneously support cell and tissue growth, while delivering specific growth factors or drugs to target a particular disease, or to serve as models to test the efficacy of drugs in 3D cell models. The scaffolds can also protect the drug against environmental factors such as moisture, temperature or pH, which can comprise its therapeutic efficacy [117]. As mentioned above, a simple way to process polymers while preserving the bioactivity of entrapped drugs, growth factors or other relevant biomolecules is the use of supercritical CO_2, so as to avoid the use of toxic solvents and high temperatures required for polymer melting. In an interesting example, chitosan-chondroitin sulfate nanoparticles were loaded with platelet lysate, an autologous source of growth factors (GFs) that provides several bioactive agents that promote bone regeneration, and then incorporated into PLA scaffolds produced by SCFs foaming [118]. In a similar direction, Kanczler et al. prepared PLA-based scaffolds for the encapsulation of vascular endothelial growth factor-165 (VEGF) to prove that the release of GFs can stimulate the development of therapeutic neovascularisation [119]. A continuation of this work tackled bone regeneration by PLA scaffolds containing VEGF with human bone marrow stromal cells (hBMSC), implanted in a mouse femur segmental defect [120]. One of the main challenges in tissue engineering is related to vascularization within artificial scaffolds, and in the case of bone adequate blood supply is key toward a successful implant. Therefore, the incorporation of VEGF to modulate angiogenesis might address vascularization during bone repair. The presence of VEGF within scaffolds seeded with hBMSC resulted in significant bone regeneration, as compared to bare PLA scaffolds.

Bioactive glasses that can stimulate osteoblast proliferation and act as angiongenic factors, have also been incorporated within PLGA scaffolds for bone tissue engineering [121]. Such bioactive glasses can act as nucleation agents during foaming under supercritical conditions, thereby affecting pore formation, and have been explored as an alternative to the incorporation of GFs. The sustained release of bioactive lipids, together with calcium and silicon ions was shown to enhance biological activities such as adhesion, proliferation and osteogenic differentiation of rat bonemarrow-derived mesenchymal stem cells (rBMSCs), as well as the proliferative and *in vitro* angiogenic ability of human umbilical vein endothelial cells (hUVECs). *In vivo* analysis of the critical-sized rat calvarial bone defect model demonstrated that the scaffolds improved vascularized bone regeneration.

4.2. Neural cell growth

In order to fully understand how information is exchanged in the human brain, the study of synaptic interactions in the neuronal network is required, where neurons are to be localized in a 3D environment [122]. Current *in vivo* studies make use of animal models, which are poorly related to the human brain, while most *in vitro* techniques are still limited to unrealistic 2D planar cell culture systems [42]. Modern neuroscience is thus in need of novel scaffolds that can support neuronal differentiation while allowing the formation of the synaptic construct, to mimic a natural neuronal network. Research in this respect has focused on the implementation of biocompatible constructs to guide embryonic cells toward differentiation and growth of neuronal circuits [123]. However, the recreated networks lack a suitable 3D architecture, thus limiting the number of formed synapsis and hindering the communication of the overall neuronal system. To overcome these limitations, engineered 3D porous scaffolds have been recently used to achieve a spatially controlled synaptic neuronal system to obtain further insight into the signaling present in natural central nervous systems [122].

Inverse opals have been considered as support scaffolds for neuronal studies, again due to their ordered interconnected porosity [25]. The ordered structure of IOs facilitated studies on the effect of matrix chemical composition on nerve regeneration and tissue differentiation. As an example, Kuo et al. studied the viability of a polymer colloidal crystal composed of three different polymers [124]. By varying the polymer composition of the porous matrix, differences in cell adhesion, viability and stability of the solid support were observed, so that the impact of each individual component on the whole system could be understood. This study demonstrated that the overall biocompatibility of a scaffold not only depends on the chemical affinity but also on the mechanical properties of the porous matrix. Other works from the same group showed improved biocompatibility by functionalizing the pore surface with biomolecules (**Figure 13**) [125–128]. By loading additional functional groups cell growth and differentiation were induced further, in comparison with nude scaffold, which highlights the importance of the interactions between cells and the functional surface of the empty cavities. This technique opens up the path for a wide range of materials to be used as scaffolding materials, as biocompatibility can always be further improved by post-synthesis functionalization.

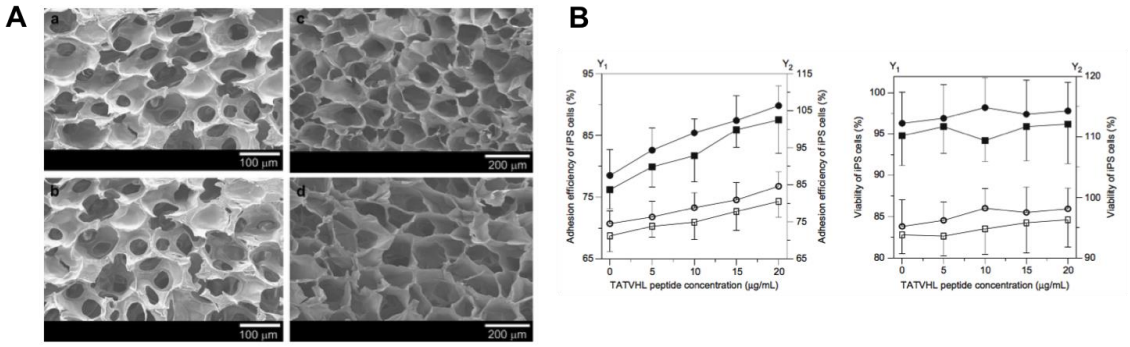

Figure 13. A) SEM images of alginate/poly(γ-glutamic acid) (γ-PGA ICC (a,b) and freeform scaffolds (c,d) with 1% (w/w) Ca. Ratios of alginate/γ-PGA: 2:3 (a,c); 3:2, (b,d). B) Adhesion efficiency and viability (respectively) of induced pluripotent stem cells (iPs) cultured in TATVHL peptide-grafted alginate/γ-PGA scaffolds. (●) ICC, alginate/ γ-PGA = 2:3 (a); (■) ICC, alginate/ γ-PGA =3:2 (c); (○) freeform alginate/ γ-PGA =2:3 (b); (□) freeform alginate/ γ-PGA =3:2 (d). Adapted with permission from ref. 125. Copyright © 2012 Elsevier.

HIPE-templated porous matrices have been also tested for neuronal tissue engineering. In a work by Murphy et al., a comparison of different thiol-ene photo-polymerized materials was carried out to study their impact on the development of a neuronal network over a 3-day culture [129]. Through diverse staining techniques, neural precursor cells (NPC) were observed in all scaffolds. The effect of the supporting scaffold on the maturation of the cultured cells was monitored through the expression of vimentin, an intermediate filament protein present during the development of the central nervous system [130]. Subsequent staining results demonstrated the ability of all matrices to induce neural differentiation. To demonstrate the importance of the mechanical properties of the support structure toward long-term cell differentiation, a second work from the same group investigated the influence of a poly(ethylene glycol) diacrylate (PEGDA) poly-HIPE scaffold on the growth of two different neuronal cell lines (**Figure 14**) [42]. To verify the obtained results, the scaffold was compared with other poly-HIPE scaffolds of similar morphology but with diverse elastic and storage moduli. Over a period of 14 days, although PEGDA scaffolds showed limitations regarding cell imaging ability, they proved to be able to promote cell adhesion and differentiation faster than other comparable hydrogels, as their mechanical properties were prepared to be as similar as possible to that of mammalian brain tissue.

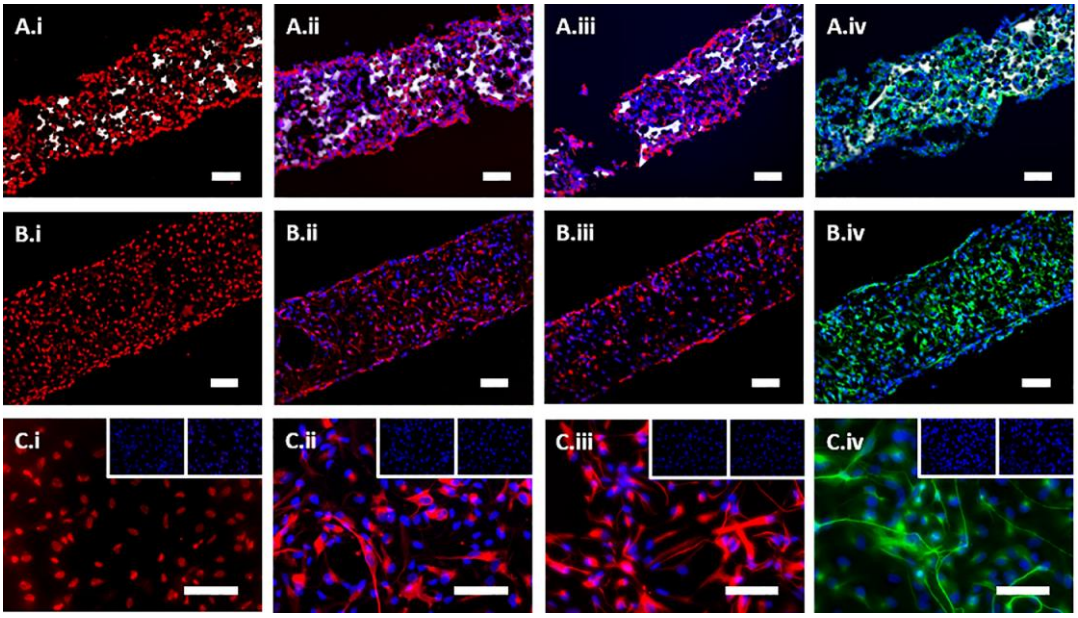

Figure 14. Immunocytochemical detections of early neural protein markers in human induced pluripotent stem cells derived from neural precursor cells hiPSC-NPCs cultured in PEG-diacrylate (PEGDA) and trimethylolpropane triacrylate (TMPTA) polyHIPE scaffolds for 14 days: A) PEGDA polyHIPE scaffolds, B) TMPTA polyHIPE scaffolds and C) 2D control-glass slides. The staining are: i) SOX1 detected with AF568 (red), ii) VIMENTIN with AF568 (red), iii) NESTIN with AF568 (red),, iv) βIII-Tubulin with AF488 (green). Reproduced with permission from ref. 42 © 2019 Acta Materialia Inc. Published by Elsevier.

The ISISA approach has also been applied to the preparation of scaffolds for neural cell growth. Using this technique, free-standing, porous and flexible 3D graphene oxide (GOx)-based scaffolds were prepared with 80% porosity, uniform layer thickness of 100-120 µm, and pore dimensions from 150 to 180 µm in length and 40 µm in width [131]. Aqueous GOx suspensions were processed by ISISA and subsequently crosslinked using hexamethylene diisocyanate to reinforce the network. A thermal treatment (200 °C for 30 min) was then applied and the scaffolds were coated with poly-lysine. Their use for neural repair was evaluated by exploring the behavior of embryonic neural progenitor cells (ENPCs) on the 3D substrates (**Figure 15**). Limited colonization was observed within the scaffolds, around 50 µm in depth, and neural cell growth and maturation were supported for 14 days *in vitro*. Interconnected neural networks conformed by both neurons and glial cells were obtained in the scaffolds, along with dendrites, axons and synaptic connections. The authors attributed the equal differentiation of ENPCs toward both neurons and glial cells, to the higher adsorption of proteins within the scaffold because of a higher content of oxygenated functional groups compared to previously reported graphene-based substrates.

In view of the potential of carbon-based 3D scaffolds for cell growth and neural tissue repair, del Monte and co-workers explored their cytocompatibility for three types of mammalian cells (murine fibroblasts, human bone sarcoma cells and porcine endothelial progenitor cells). Time-lapse confocal laser scanning microscopy was employed for the first time to study cell migration processes in real time, within these 3D scaffolds [132]. The chemical nature of the polymers (chitosan, chondroitin sulfate, gelatin), the temperature of the ISISA treatment and the type of MWCNTs affected the porosity and surface roughness of the scaffolds. The scaffold architecture and morphology were found to be responsible for cell behavior. The highest viability was observed for scaffolds with a pore size similar to that of cells, and with lower surface roughness. The presence of MWCNTs was reported to not affect cell adhesion and morphology, so that the cells were mostly suspended in air, within pore spaces between walls. Therefore, if the size of the pore was comparable to that of the cells, contact points between cells and scaffold would be minimized. The results revealed that suitable cell-material interactions depend on material- and cell-dependent parameters, so optimization is required in every case. As a general rule, by minimizing the contact points between cells and scaffold, as well as surface roughness of the material, cell viability is improved.

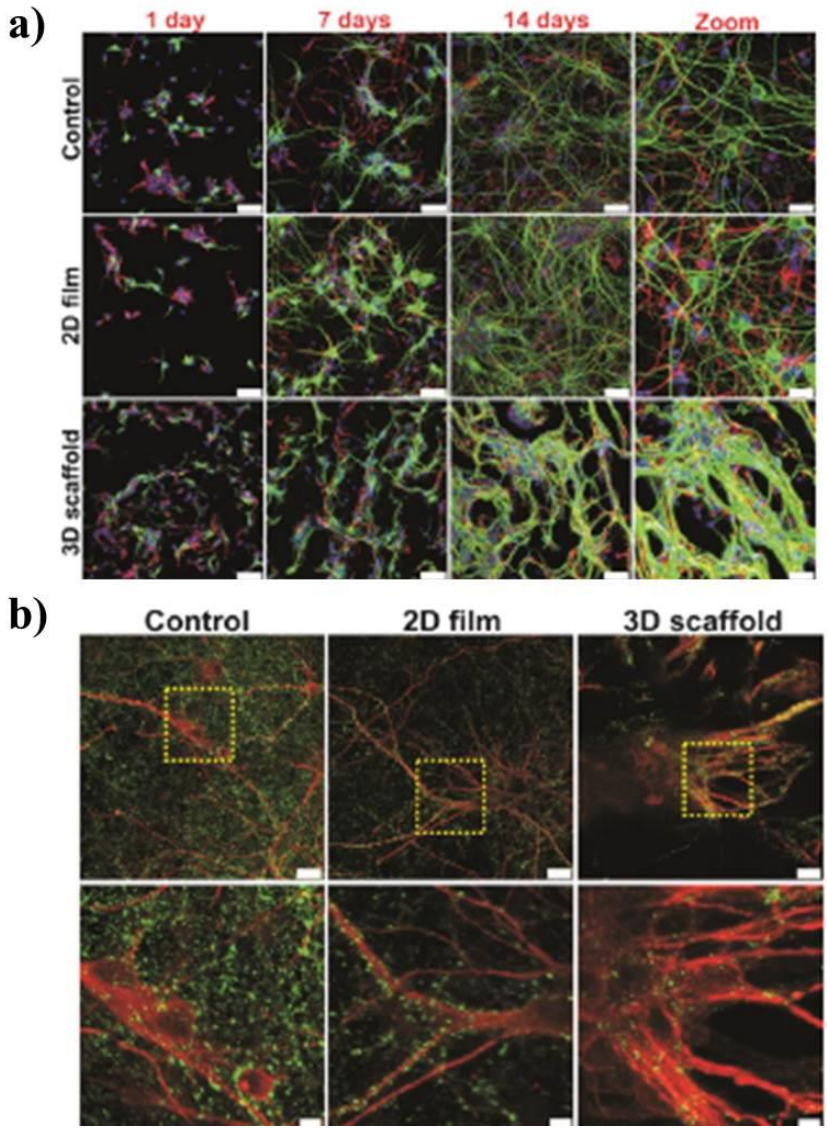

Figure 15. (a) ENPC differentiation studies on graphene oxide-based substrates over time. CLSM images showing staining for map-2 (green), vimentin (red) and cell nuclei (blue) at different time points (scale bars are 50 μm, scale bars in zoom images are 25 μm). (b) Synapsis formation on the substrates. CLSM images showing staining for synaptophysin (green) and map-2 (red) at 14 days (scale bars are 25 μm for top images, 10 μm for bottom images in control, and 7.5 μm in 2D film and 3D scaffold). Adapted from ref. 131 with permission from the Royal Society of Chemistry.

Taking into account these results, Gutierrez et al. explored the use of chondroitin sulfate-based 3D scaffolds containing MWCNTs for nervous tissue repair (**Figure 16**) [133]. These scaffolds featured an estimated pore area of 51% and an averaged pore width of 8.9 μm. A significant result was the formation of viable cultures enriched in neuron cells for up to 20 days, with the ability to display calcium transients and active mitochondria potential, even in the absence of poly-lysine coating, which was not the case for 2D substrates. The 3D structure of the scaffold appeared to protect the

embryonic neural progenitor cells as compared to 2D cultures, while cell viability was supported up to 20 days within 3D scaffolds. It is worth mentioning the importance of developing new imaging and analytical tools for the study of complex 3D cell models as, in this case, the number and length of neurites including axons per surface unit could not be monitored over time, due to the complex 3D architecture of the substrate.

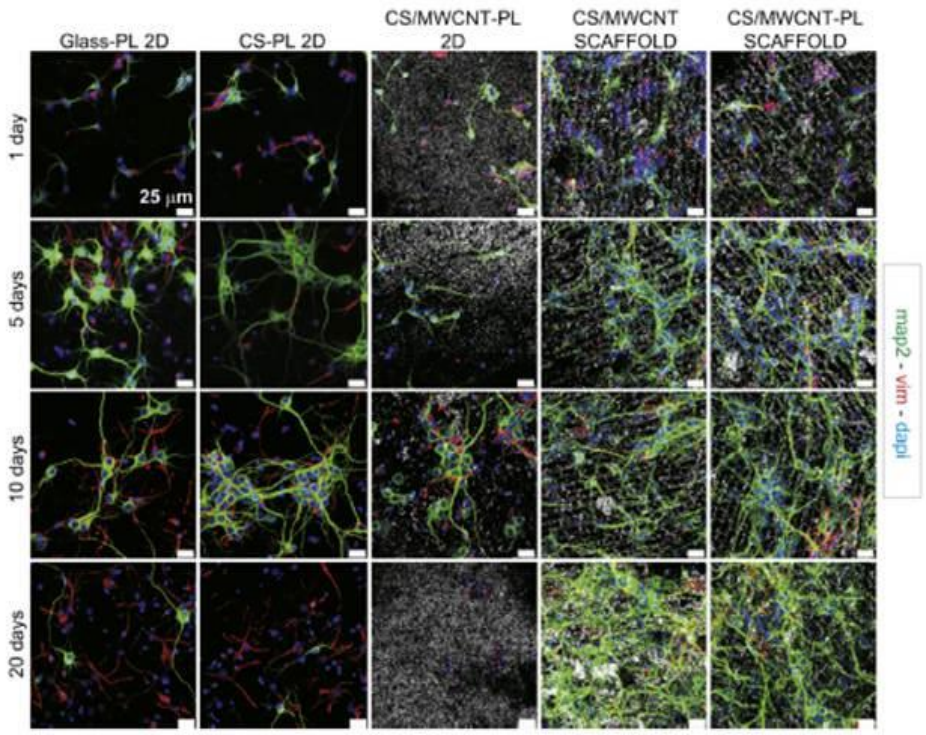

Figure 16. ECNP differentiation studies on MWCNTs/chondroitin sulfate substrates. Representative CLSM images showing staining for map-2 (green), vimentin (red) and cell nuclei (blue) in different cell cultures. The reflection of the substrates containing MWCNTs can be observed to reveal substrate architecture. Scale bars represent 25 μm in all images. Reprinted with permission from ref. 133. Copyright © 2013 Elsevier.

4.3. Cardiac tissue and neovascularization

The heart is known to be one of the most important organs in the human body, for its capacity to recycle and pump blood to all other organs. Cardiac engineering has progressed toward the fabrication of functional cardiac tissues through the use of artificial scaffolds that mimic the biological complexity of the required environment [134]. However, the biological mechanisms for heart tissue building need to fulfil some requirements that remain challenging for current tissue-engineering approaches. For example, it is important to introduce factors affecting the organization of the precursor cardiac cells (known as cardiomyocytes) or to achieve synchronized beating [135,136].

To study such diverse parameters, solid porous structures are required to support tissue growth while allowing the diffusion of oxygen and other factors required for cell growth and differentiation [25]. Efforts have been made to enlighten the relationship between pore size, shape and interconnected channels in porous scaffolds and the growth of cardiac tissue [137]. Most of the studies related to the use of IO for cardiac tissue engineering attempted to correlate the impact of pore size to the growth of new blood vessels. Several *in vitro* studies proved the existence of size thresholds that define the density and thickness of the new blood vessels [137,138]. Pores smaller than 200 μm favor the formation of smaller vessels in higher density, whereas bigger cavities induced a reduction in the amount of formed vessels, promoting increased diffusion (**Figure 17**) [139,140]. Notwithstanding, excessively large pores would be unable to retain control over the interactions between cardiac cells due to far distancing, thus impeding the formation of new vessels. In a closer *in vivo* approach, Madden et al. studied the neovascularization and fibrous encapsulation by implanting diverse collagen-modified poly(2-hydroxyethyl methacrylate-co-methacrylic acid) scaffolds (with pores ranging from 20 to 80 μm) into the myocardium of immunocompetent rats [141]. After a 4 week time period, differences in the density of perfused vessels led to the conclusion that smaller pores achieved maximum vascularization while minimizing fibrous encapsulation. To explain the observed differences in neovascularization, variances in the phenotype of the interiorized cells were evaluated, concluding that an increase in neovascularization was promoted by the size of the pores inducing a shift towards prohealing, thereby enhancing the required vascularization.

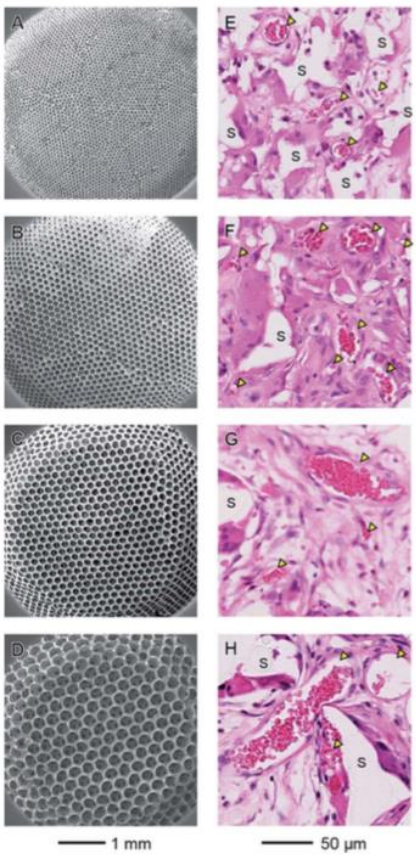

Figure 17. (A-D) SEM of PLGA inverse opals with pore sizes of 79, 147, 224 and 312 µm, respectively. (E-H) Bright field images representative of hematoxylin- and eosin-stained sections of the surface of each respective scaffold 4 weeks post-implantation. The areas marked with "S" correspond to the scaffold, while the yellow arrowheads indicate blood vessels. Reproduced from ref. 140 with permission from the Royal Society of Chemistry.

5. CONCLUSIONS AND OUTLOOK

Although porous scaffolds for tissue engineering have been around for quite a long time, the field is still blossoming, as new materials and techniques are developed. We have reviewed selected (colloid-oriented) fabrication methods toward 3D porous scaffolds with well-organized microstructures, as well as relevant applications thereof. In our view, the ideal scaffold should possess suitable pore size and porosity to promote cell-matrix and cell-cell interactions, as well as interconnected porosity to facilitate cell diffusion, and transport of nutrients and oxygen. Excellent advances in scaffold fabrication techniques already provide control over the above mentioned parameters, while offering the possibility to achieve scaffolds with gradient porosity and specific morphologies. Special attention should be paid to reducing the use of toxic chemicals, such as surfactants or harmful solvents that can damage cells and reduce the overall

biocompatibility of the scaffold. Along with the fabrication technology, modulating the material composition enables tuning scaffold degradability, mechanical properties, bioactivity and biocompatibility for the target application. It is also quite obvious that targeted delivery of regulatory biomolecules or therapeutics will further benefit tissue development.

Concerning applicability, porous 3D scaffolds are generally aimed at tissue engineering or drug delivery applications. Besides optimized porosity, the mechanical properties and morphology of the scaffolds determine their suitability for each particular case of tissue regeneration. Specific materials or growth factors can be also incorporated, either before or after fabrication, to promote cell-differentiation into the targeted tissue. An important challenge in tissue engineering is to achieve vascularization within the artificial support and to provide the required blood supply for a successful implant. Drug encapsulation and sustained release from porous scaffolds over long periods of time are also possible, opening the way to disease treatment or drug screening within *in vitro* 3D models. The scaffold must ensure cell attachment and proliferation, but in most cases, cell migration deep into the 3D network can hardly be achieved and challenges remain to ensure nutrient diffusion deeper inside the material and cell proliferation beyond a few layers.

Despite of the continuous development of fabrication techniques to create scaffolds with ever-increasing sophisticated structures, we propose that future research should head toward the development of imaging tools which maintain high spatial and temporal resolution to monitor cellular events within the whole volume of the scaffold. As mentioned previously, one of the main challenges faced when dealing with 3D scaffolds is to study cellular processes far from the surface of the material. Up to date, confocal fluorescence microscopy has generally been the technique of choice for cell imaging. However, this technique is still hindered by a limited penetration depth, and thus minimally invasive high resolution techniques with increased penetration depth are required for live-cell imaging within 3D scaffolds. Besides deeper penetration, other aspects such as long-term monitoring of cellular behavior in the absence of photobleaching, phototoxicity or quenching issues, will be of great importance toward a better understanding of tissue growth or disease progression. Other bioimaging options include Computed Tomography (TC), Magnetic Resonance Imaging (MRI) or Positron Emission Tomography (PET). However, their spatial resolution is still limited to 1 to 2 mm and single cell studies are not possible. Emerging techniques such as surface-

enhanced Raman scattering (SERS) spectroscopy are interesting alternatives for bioimaging due to their non-invasive nature avoiding cell-fixation, deeper light penetration for biological tissues within the NIR window and high sensitivity. Since this technique takes advantage of the plasmonic properties of noble-metal nanoparticles, the use of colloid-based approaches to the construction of porous scaffolds offers plenty of possibilities toward the use of hybrid nanocomposite materials. The analytical capability of SERS for highly specific detection of relevant analytes may facilitate the in situ detection of cell-secreted molecules and relevant biomarkers that could give important clues to understand disease progression. SERS and related techniques are expected to facilitate *in vitro* drug screening and treatment validation, thereby speeding up the translation of materials into *in vivo* models or clinical trials. Therefore, significant advances in bioimaging and bioanalytical tools related to *in situ* monitoring of cellular processes within 3D scaffolds are expected to complement the development of more realistic 3D tissue models.

DECLARATION OF COMPETING INTEREST

The authors declare no conflict of interest

ACKNOWLEDGEMENTS

The authors acknowledge financial support by the European Research Council (ERC-AdG-2017# 787510). C. G. A. thanks the Spanish State Research Agency for a Juan de la Cierva Formación Fellowship (FJCI-2016-28887). This work was performed under the Maria de Maeztu Units of Excellence Programme – Grant No. MDM-2017-0720 Ministry of Science, Innovation and Universities.

REFERENCES

[1] Huh D, Hamilton GA, Ingber DE, Trends Cell Biol, 2011;21:745–54.

[2] Yamada KM, Cukierman E, Cell, 2007;130:601–10.

[3] Salerno A, Pascual CD, Process Biochem, 2015;50:826–38.

[4] Loh QL, Choong C, Tissue Eng Part B Rev, 2013;19:485–502.

[5] Qu H, Fu H, Han Z, Sun Y, RSC Adv, 2019;9:26252–62.

[6] Zhu L, Luo D, Liu Y, Int J Oral Sci, 2020;12:1–15.

[7] Shoichet MS, Macromolecules, 2010;43:581–91.

[8] Hsu SH, Hung KC, Chen CW, J Mater Chem B, 2016;4:7493–505.

[9] Li YC, Zhang YS, Akpek A, Shin SR, Khademhosseini A, Biofabrication, 2017;9:1–16.

[10] Murphy S V., Atala A, Nat Biotechnol, 2014;32:773–85.

[11] Gungor-Ozkerim PS, Inci I, Zhang YS, Khademhosseini A, Dokmeci MR, Biomater Sci, 2018;6:915–46.

[12] Truby RL, Lewis JA, Nature, 2016;540:371–8.

[13] Dutta RC, Dutta AK, Biotechnol Adv, 2009;27:334–9.

[14] Williams DF, Biomaterials, 2008;29:2941–53.

[15] Deb P, Deoghare AB, Borah A, Barua E, Das Lala S, Mater. Today Proc., vol. 5, Elsevier Ltd; 2018, p. 12909–19.

[16] Sgarminato V, Tonda-Turo C, Ciardelli G, J Biomed Mater Res - Part B Appl Biomater, 2020;108:1176–85.

[17] Carletti E, Motta A, Migliaresi C, Methods Mol Biol, 2011;695:17–39.

[18] Bose S, Roy M, Bandyopadhyay A, Trends Biotechnol, 2012;30:546–54.

[19] B G, B L, P L, PX M, Regen Biomater, 2015;2.

[20] Nikolova MP, Chavali MS, Bioact Mater 2019;4:271–92.

[21] Alvarez K, Nakajima H, Materials (Basel), 2009;2:790–832.

[22] Hollister SJ, Adv Mater, 2009;21:3330–42.

[23] Olszta MJ, Cheng X, Jee SS, Kumar R, Kim YY, Kaufman MJ, Douglas EP, Gower LB, Mater Sci Eng R Reports, 2007;58:77–116.

[24] Bramfeld H, Sabra G, Centis V, Vermette P, Curr Med Chem, 2010;17:3944–67.

[25] João CFC, Vasconcelos JM, Silva JC, Borges JP, Tissue Eng Part B Rev, 2014;20:437–54.

[26] Mishchenko L, Hatton B, Kolle M, Aizenberg J, Small, 2012;8:1904–11.

[27] van Blaaderen A, Science, 1998;282:887–888.

[28] Lange B, Metz N, Tahir MN, Fleischhaker F, Theato P, Schröder H-C, Müller VEG, Tremel W, Zentel R, Macromol Rapid Commun, 2007;28:1987–94.

[29] Li X, Yu J, Jaroniec M. Surface Science of Photocatalysis. Interface Sci Technol, vol. 31, Elsevier; 2020.Chapter 3.

[30] Armstrong E, O'Dwyer C, J Mater Chem C, 2015;3:6109–43.

[31] Aguirre CI, Reguera E, Stein A, Adv Funct Mater, 2010;20:2565–78.

[32] Lima MJ, Correlo VM, Reis RL, Mater Sci Eng C, 2014;42:615–21.

[33] Zhang YS, Zhu C, Xia Y, Adv Mater, 2017;29:1701115.

[34] Zhang YS, Regan KP, Xia Y, Macromol Rapid Commun, 2013;34:485–91.

[35] Meseguer F, Blanco A, Míguez H, García-Santamaría F, Ibisate M, López C, Colloids Surfaces A Physicochem Eng Asp, 2002;202:281–90.

[36] Velev OD, Lenhoff AM, Curr Opin Colloid Interface Sci, 2000;5:56–63.

[37] Carpenter R, Macres D, Kwak J-G, Daniel K, Lee J, Tissue Eng Part C Methods, 2020;26:143–55.

[38] Kuai S-L, Truong V-V, Haché A, Hu X-F, J Appl Phys, 2004;96:5982–6.

[39] Stein A, Li F, Denny NR, Chem Mater, 2008;20:649–66.

[40] Pulko I, Krajnc P, Macromol Rapid Commun, 2012;33:1731–46.

[41] Owen R, Sherborne C, Paterson T, Green NH, Reilly GC, Claeyssens F, J Mech Behav Biomed Mater, 2016;54:159–72.

[42] Murphy AR, Haynes JM, Laslett AL, Cameron NR, O'Brien CM, Acta Biomater, 2020;101:102–16.

[43] Sgarminato V, Tonda-Turo C, Ciardelli G, J Biomed Mater Res Part B Appl Biomater, 2020;108:1176–85.

[44] Cameron NR, Polymer, 2005;46:1439–49.

[45] Williams JM, Wrobleski DA, Langmuir, 1988;4:656–62.

[46] Luo W, Zhang S, Li P, Xu R, Zhang Y, Liang L, Wood CD, Lu Q, Tan B, Polymer, 2015;61:183–91.

[47] Cameron NR, Sherrington DC, Albiston L, Gregory DP, Colloid Polym Sci, 1996;274:592–5.

[48] Barbetta A, Cameron NR, Cooper SJ, Chem Commun, 2000:221–2.

[49] Kirkpatrick FH, Gordesky SE, Marinetti GV, Biochim Biophys Acta – Biomembr, 1974;345:154–61.

[50] Yang Y, Fang Z, Chen X, Zhang W, Xie Y, Chen Y, Liu Z, Yuan W, Front Pharmacol, 2017;8:287.

[51] Zhu Y, Huan S, Bai L, Ketola A, Shi X, Zhang X, Ketoja JA, Rojas OJ, ACS Appl Mater Interfaces, 2020;12:11240–51.

[52] Lee J, Chang JY, Chem Eng J, 2020;381:122767.

[53] Luo W, Xu R, Liu Y, Hussain I, Lu Q, Tan B, RSC Adv, 2015;5:92017–24.

[54] Palocci C, Barbetta A, La Grotta A, Dentini M, Langmuir, 2007;23:8243–51.

[55] Chen K, Grant N, Liang L, Zhang H, Tan B, Macromolecules, 2010;43:9355–64.

[56] Beckman EJ, J Supercrit Fluids, 2004;28:121–91.

[57] Gutiérrez MC, García-Carvajal ZY, Jobbágy M, Rubio F, Yuste L, Rojo F, Ferrer ML, del Monte F, Adv Funct Mater, 2007;17:3505–13.

[58] Gutiérrez MC, García-Carvajal ZY, Hortigüela MJ, Yuste L, Rojo F, Ferrer ML, del Monte F, J Mater Chem, 2007;17:2992–5.

[59] Deville S, Saiz E, Tomsia AP, Biomaterials, 2006;27:5480–9.

[60] Poursamar SA, Azami M, Mozafari M, Colloids Surfaces B Biointerfaces, 2011;84:310–6.

[61] Zhang H, Hussain I, Brust M, Butler MF, Rannard SP, Cooper AI, Nat Mater, 2005;4:787–93.

[62] Gutiérrez MC, Ferrer ML, Del Monte F, Chem Mater, 2008;20:634–48.

[63] Deville S, Saiz E, Nalla RK, Tomsia AP, Science, 2006;311:515–8.

[64] Ghosh D, Dhavale N, Banda M, Kang H, Ceram Int, 2016;42:16138–47.

[65] Naglieri V, Bale HA, Gludovatz B, Tomsia AP, Ritchie RO, Acta Mater, 2013;61:6948–57.

[66] Deville S, J Mater Res, 2013;28:2202–19.

[67] Mukai SR, Nishihara H, Tamon H, Chem Commun, 2004;4:874–5.

[68] Nishihara H, Mukai SR, Fujii Y, Tago T, Masuda T, Tamon H, J Mater Chem, 2006;16:3231–6.

[69] Hortigüela MJ, Aranaz I, Gutiérrez MC, Ferrer ML, Del Monte F, Biomacromolecules, 2011;12:179–86.

[70] Ferrer ML, Esquembre R, Ortega I, Reyes Mateo C, Del Monte F, Chem Mater, 2006;18:554–9.

[71] Gutiérrez MC, Hortigüela MJ, Manuel Amarilla J, Jiménez R, Ferrer ML, Del Monte F, J Phys Chem C, 2007;111:5557–60.

[72] Gutiérrez MC, García-Carvajal ZY, Jobbágy M, Yuste L, Rojo F, Abrusci C, Catalina F, del Monte F, Ferrer ML, Chem Mater, 2007;19:1968–73.

[73] Nieto M, Nardecchia S, Peinado C, Catalina F, Abrusci C, Gutiérrez MC, Ferrer ML, del Monte F, Soft Matter, 2010;6:3533–40.

[74] Guan LZ, Gutiérrez MC, Roldán-Ruiz MJ, Jiménez R, Ferrer ML, del Monte F, Adv Mater, 2019;31:1903418.

[75] Gutiérrez MC, Jobbágy M, Ferrer ML, Del Monte F, Chem Mater, 2008;20:11–3.

[76] Gutiérrez MC, Jobbágy M, Rapún N, Ferrer ML, del Monte F, Adv Mater, 2006;18:1137–40.

[77] Christoph S, Kwiatoszynski J, Coradin T, Fernandes FM, Macromol Biosci, 2016;16:182–7.

[78] Nishihara H, Mukai SR, Yamashita D, Tamon H, Chem Mater, 2005;17:683–9.

[79] Rajamanickam R, Kumari S, Kumar D, Ghosh S, Kim JC, Tae G, Gupta SS, Kumaraswamy G, Chem Mater, 2014;26:5161–8.

[80] Salerno A, Zeppetelli S, Maio E Di, Iannace S, Netti PA, Compos Sci Technol, 2010;70:1838–46.

[81] Salerno A, Diéguez S, Diaz-Gomez L, Gómez-Amoza JL, Magariños B, Concheiro A, Domingo C, Alvarez-Lorenzo C, García-González CA, Biofabrication, 2017;9:35002.

[82] Diaz-Gomez L, Concheiro A, Alvarez-Lorenzo C, García-González CA, Carbohydr Polym, 2016;142:282–92.

[83] Fanovich MA, Ivanovic J, Misic D, Alvarez M V., Jaeger P, Zizovic I, Eggers R, J Supercrit Fluids, 2013;78:42–53.

[84] Salerno A, Fanovich MA, Pascual CD, J Supercrit Fluids 2014;95:394–406.

[85] Fanovich MA, Jaeger P, Mater Sci Eng C, 2012;32:961–8.

[86] Mou ZL, Zhao LJ, Zhang QA, Zhang J, Zhang ZQ, J Supercrit Fluids, 2011;58:398–406.

[87] Tsivintzelis I, Pavlidou E, Panayiotou C, J Supercrit Fluids, 2007;42:265–72.

[88] Kiran E, J. Supercrit. Fluids, 2010; 54: 296–307.

[89] Salerno A, Domingo C, Microporous Mesoporous Mater, 2014;184:162–8.

[90] Salerno A, Fernández-Gutiérrez M, San Román Del Barrio J, Domingo C, J Supercrit Fluids, 2015;97:238–46.

[91] Salerno A, Fernández-Gutiérrez M, San Román Del Barrio J, Pascual CD, RSC

Adv, 2014;4:61491–502.

[92] Salerno A, Domingo C, J Supercrit Fluids, 2019;143:146–56.

[93] Collins NJ, Bridson RH, Leeke GA, Grover LM, Acta Biomater, 2010;6:1055–60.

[94] Bhamidipati M, Scurto AM, Detamore MS, Tissue Eng Part B Rev, 2013;19:221–32.

[95] Reverchon E, Cardea S, J Supercrit Fluids, 2012;69:97–107.

[96] Harris LD, Kim B, Mooney DJ, J Biomed Mater Res, 1998;42:396–402.

[97] Salerno A, Domingo C, Polym Int, 2014;63:1303–10.

[98] Salerno A, Saurina J, Domingo C, Int J Pharm, 2015;496:654–63.

[99] Ji C, Annabi N, Khademhosseini A, Dehghani F, Acta Biomater, 2011;7:1653–64.

[100] Annabi N, Mithieux SM, Weiss AS, Dehghani F, Biomaterials, 2009;30:1–7.

[101] Tsioptsias C, Panayiotou C, J Supercrit Fluids, 2008;47:302–8.

[102] Tsioptsias C, Paraskevopoulos MK, Christofilos D, Andrieux P, Panayiotou C, Polymer, 2011;52:2819–26.

[103] Annabi N, Mithieux SM, Weiss AS, Dehghani F, Biomaterials, 2010;31:1655–65.

[104] Gong T, Xie J, Liao J, Zhang T, Lin S, Lin Y, Bone Res, 2015;3:15029.

[105] Hollister SJ, Nat Mater, 2005;4:518–24.

[106] Kanczler JM, Wells JA, Gibbs DMR, Marshall KM, Tang DKO, Oreffo ROC. Principles of Tissue Engineering Elsevier; 2020, Chapter 50.

[107] João C, Almeida R, Silva J, Borges J, Mater Lett, 2016;185:407–10.

[108] Cuddihy MJ, Kotov NA, Tissue Eng Part A, 2008;14:1639–49.

[109] Choi S-W, Zhang Y, Thomopoulos S, Xia Y, Langmuir, 2010;26:12126–31.

[110] Hu Y, Cao S, Chen J, Zhao Y, He F, Li Q, Zou L, Shi C, Chem Eng J, 2020;394:124895.

[111] Paljevac M, Gradišnik L, Lipovšek S, Maver U, Kotek J, Krajnc P, Macromol Biosci, 2018;18:1700306.

[112] Abarrategi A, Gutiérrez MC, Moreno-Vicente C, Hortigüela MJ, Ramos V, López-Lacomba JL, Ferrer ML, del Monte F, Biomaterials, 2008;29:94–102.

[113] Hortigüela MJ, Gutiérrez MC, Aranaz I, Jobbágy M, Abarrategi A, Moreno-Vicente C, Civantos A, Ramos V, López-Lacomba JL, Ferrer ML, del Monte F, J Mater Chem, 2008;18:5933–40.

[114] Fonseca-García A, Mota-Morales JD, Quintero-Ortega IA, García-Carvajal ZY, Martínez-López V, Ruvalcaba E, Landa-Solís C, Solis L, Ibarra C, Gutiérrez MC, Terrones M, Sanchez IC, del Monte F, Velasquillo MC, Luna-Bárcenas G, J Biomed Mater Res Part A, 2014;102:3341–51.

[115] Bai H, Wang D, Delattre B, Gao W, De Coninck J, Li S, Tomsia AP, Acta Biomater, 2015;20:113–9.

[116] White LJ, Hutter V, Tai H, Howdle SM, Shakesheff KM, Acta Biomater, 2012;8:61–71.

[117] Fenton OS, Olafson KN, Pillai PS, Mitchell MJ, Langer R, Adv Mater, 2018;30:1705328.

[118] Santo VE, Duarte ARC, Popa EG, Gomes ME, Mano JF, Reis RL, J Control Release, 2012;162:19–27.

[119] Kanczler JM, Barry J, Ginty P, Howdle SM, Shakesheff KM, Oreffo ROC, Biochem Biophys Res Commun, 2007;352:135–41.

[120] Kanczler JM, Ginty PJ, Barry JJA, Clarke NMP, Howdle SM, Shakesheff KM, Oreffo ROC, Biomaterials, 2008;29:1892–900.

[121] Li S, Song C, Yang S, Yu W, Zhang W, Zhang G, Xi Z, Lu E, Acta Biomater, 2019;94:253–67.

[122] Bosi S, Rauti R, Laishram J, Turco A, Lonardoni D, Nieus T, Prato M, Scaini D,

Ballerini L, Sci Rep, 2015;5:9562.

[123] Murphy AR, Laslett A, O'Brien CM, Cameron NR, Acta Biomater, 2017;54:1–20.

[124] Kuo YC, Lin CC, Colloids Surfaces B Biointerfaces, 2013;103:595–600.

[125] Kuo YC, Chung CY, Biomaterials, 2012;33:8955–66.

[126] Kuo YC, Wang CC, Colloids Surfaces B Biointerfaces, 2013;104:194–9.

[127] Kuo YC, Chiu KH, Biomaterials, 2011;32:819–31.

[128] Yang JT, Kuo YC, Chiu K-H, Colloids Surfaces B Biointerfaces, 2011;84:198–205.

[129] Murphy AR, Ghobrial I, Jamshidi P, Laslett A, O'Brien CM, Cameron NR, Polym Chem, 2017;8:6617–27.

[130] Pérez-Álvarez MJ, Isiegas C, Santano C, Salazar JJ, Ramírez AI, Triviño A, Ramírez JM, Albar JP, de la Rosa EJ, Prada C, J Neurosci Res, 2008;86:1871–83.

[131] Serrano MC, Patiño J, García-Rama C, Ferrer ML, Fierro JLG, Tamayo A, Collazos-Castro JE, del Monte F, Gutiérrez MC, J Mater Chem B, 2014;2:5698–706.

[132] Nardecchia S, Serrano MC, Gutiérrez MC, Ferrer ML, Del Monte F, J Mater Chem B, 2013;1:3064–72.

[133] Serrano MC, Nardecchia S, García-Rama C, Ferrer ML, Collazos-Castro JE, Del Monte F, Gutiérrez MC, Biomaterials, 2014;35:1543–51.

[134] Zhang YS, Aleman J, Arneri A, Bersini S, Piraino F, Shin SR, Dokmeci MR, Khademhosseini A, Biomed Mater, 2015;10:034006.

[135] Ahmed M, Yildirimer L, Khademhosseini A, Seifalian AM, J Nanosci Nanotechnol, 2012;12:4775–85.

[136] Camci-Unal G, Annabi N, Dokmeci MR, Liao R, Khademhosseini A, NPG Asia Mater, 2014;6:e99.

[137] Feng B, Jinkang Z, Zhen W, Jianxi L, Jiang C, Jian L, Guolin M, Xin D, Biomed Mater, 2011;6:015007.

[138] Ye X, Lu L, Kolewe ME, Hearon K, Fischer KM, Coppeta J, Freed LE, Adv Mater, 2014;26:7202–8.

[139] Choi S-W, Zhang Y, MacEwan MR, Xia Y, Adv Healthc Mater, 2013;2:145–54.

[140] Zhang YS, Choi SW, Xia Y, Soft Matter, 2013;9:9747–54.

[141] Madden LR, Mortisen DJ, Sussman EM, Dupras SK, Fugate JA, Cuy JL, Hauch KD, Laflamme MA, Murry CE, Ratner BD, Proc Natl Acad Sci, 2010;107:15211–6.